Ph.D. Dissertation

International Doctoral School in Information and Communication Technology

DISI - University of Trento

Innovative Strategies for the Synthesis of Time Modulated Antenna Systems

Luca Manica

Advisor:
Andrea Massa, Professor
Università degli Studi di Trento

March 2010

Acknowledgements

I would like to thank the whole Eledia group for this unforgettable experience of work and life.

I thank all the friends, teachers and colleagues I met during my PhD.

A particular thank goes to Takenaka sen-sei, Matsuda sen-sei, Tsuji sen-sei, Moriyama san and Kismet san for their kindness and hospitality during my staying at the Nagasaki University.

I also thank Prof. F. Ares for his suggestions and indications which significantly improved this work. Moreover, his outstanding research in the framework of time-modulated array mainly inspires this thesis.

The greatest thank is for my family and for Silvia.

Abstract

In the framework of the synthesis of time-modulated array antennas for communication purposes, the thesis focuses on the analysis and the development of innovative approaches aimed at reducing the power losses related with the undesired harmonic radiations. The accurate analysis of the problem in hand has been used to identify the foundamental parameters involved in the waste of power when the elements of the array are modulated using RF switches. The sideband radiations have been firstly "indirectly" handled throughout the reduction of the sideband levels of the patterns of the harmonics by means of the minimization of a suitable cost function using a stochastic optimizer, the Particle Swarm Optimizer. Successively, by exploiting a closed form relationship describing the total power wasted in sideband radiations a new synthesis method has been developed allowing a significant reduction of the computation effort and a more effective dealing with the synthesis problem. Moreover, a careful study of the potentialities and the applications of such methods in others antenna synthesis problem has been carried out referring in particular to the reduction of the sideband radiations in monopulse array antennas in which the difference pattern is obtained by means of sub-arrayed feed network. In the numerical validation, a set of representative examples concerned with the reduction of the sideband levels and the power of the harmonic radiations are reported in order to assess the effectiveness and the flexibility of the proposed approach. Comparison with previously published results are reported and discussed, as well.

Keywords
Time-Modulated Arrays, Pattern Synthesis, Particle Swarm Optimization.

Published Journal Papers

[R1] L. Manica, P. Rocca, L. Poli, and A. Massa, "Almost Time-Independent Performance in Time-Modulated Linear Arrays," *IEEE Antennas and Wireless Propagation Letter*, vol. 8, pp. 843-846, Aug. 2009.

[R2] P. Rocca, L. Manica, L. Poli, and A. Massa, "Synthesis of compromise sum-difference arrays through time-modulation," *IET Radar Sonar Navigation,* vol. 3, no. 6, pp. 630-637, Nov. 2009.

[R3] L. Poli, P. Rocca, L. Manica, and A. Massa, "Handling Sideband Radiations in Time-Modulated Arrays through Particle Swarm Optimization," *IEEE Transaction on Antennas and Propagation*, (Accepted for future publication Sept. 15 2009).

[R4] L. Poli, P. Rocca, L. Manica, and A. Massa, "Pattern Synthesis in Time-Modulated Linear Arrays through Pulse Shifting," *IET Microwave and Antenna Propagation*, (Accepted for future publication Oct. 16 2009).

[R5] L. Poli, P. Rocca, L. Manica, and A. Massa, "Time Modulated Planar Arrays - Analysis and Optimization of the Sideband Radiations," *IET Microwave and Antenna Propagation*, (Accepted for future publication Oct. 22 2009).

Published Conference Papers

[C1] P. Rocca, L. Poli, L. Manica, and A. Massa, "Compromise pattern synthesis by means of optimized time-modulated array solutions," 2009 *IEEE Antennas and Propagation Society International Symposium*, Charleston, South Carolina, USA, pp. 1-4, June 1-5, 2009.

Contents

List of Tables

List of Figures

Structure of the Thesis

The thesis is structured in chapters according to the organization detailed in the following.

The first chapter deals with an introduction of the thesis, focusing on the subject of this work as well as a presentation of the state-of-art techniques dealing with the same antenna synthesis problem.

In Chapter 2 further investigations in the framework of the synthesis of time-modulated linear arrays are presented, underling the main parameters involved in the sideband radiations, and proposing an innovative strategy, based on a global optimizer, aimed at reducing the sideband radiations optimizing the pulse shifting.

The problem of minimizing the sideband radiations is reformulated in Chapter 3. A closed relationship that computes the wasted power due to the undesired harmonics is fully exploited to deal with the problem in hand. Starting from such an expression the problem is recast as the minimization of a suitable cost function by means of the Particle Swarm Optimizer.

The extension of the approach from linear to planar time-modulated arrays is described and assessed in Chapter 4. The theory of the time-modulation is formulated to describe the behavior of the planar arrays and an explicit expression for the wasted power radiated by the undesired harmonics is derived. Successively, such a relationship is profitably used to design a new procedure based on a Particle Swarm Optimizer for the synthesis of the pulse sequences devoted to control the time-modulated array.

In Chapter 5 the time-modulation has been exploited to synthetize sub-arrayed monopulse antenna radiating sum and difference beams. The static excitations of the array have been set to obtain an optimal sum pattern whereas the "best compromise" on-time durations generating the difference pattern have been computed by means of the *Contiguous Partition Method*. Moreover, the "switch-on" instants are successively optimized by means of the Particle Swarm

Optimizer reducing the wasted power due to the sideband radiations.

Conclusions and future develpments are presented in Chapter 6. Finally, an appendix gives more details regarding the development of a closed-form expression computing the power wasted by the sideband radiations in time-modulated planar arrays.

Chapter 1

Introduction and State-of-the-Art

In the introduction, the motivation of the thesis is pointed out starting from an overview of the techniques present in the state-of-art regarding the analysis and the synthesis of the time-modulated array antennas.

The use of time as an additional degree of freedom in array synthesis has been investigated in the pioneering work by Shanks and Bickmore [1]. The essence of this philosophy is the use of the time domain as an additional variable to control the antenna radiation characteristics. Moreover, they firstly explore the potentialities of such a strategy in the multipattern operations, simultaneous scanning and sidelobe suppression. Further investigations of the use of the time-modulation had been provided in [2] where Shanks proposed a new technique to obtain electronically scanned beams for radar applications modulating the element of an array of antennas by means of rectangular pulse excitations. In such an approach, the author proposed a scheme to feed every element through a simple on-off switch made by a ferrite rotation device. Furthermore, Kummer *et al.* in [3] discussed the possibility of using RF switches for modulating in time the element excitations in order to obtain antenna patterns with average low and ultra-low side lobes.

Successivelly, even if the aforementioned strategies showed the interesting feature of reconfiguring the array pattern by simply adjusting the on-off switching sequence only few works have dealt with time-modulation (e.g., [4]). As pointed out in [3] and [5], the main difficulty to the diffusion of such a technique lie in its technical implementation. More in detail, the control feed network implementation requires RF switches realibility and robustness, able to work at very high frequency (GHz), with very small switch time and time of rise and fall ($nsec$). Additionally, in order to properly modify the antenna pattern the modulating signals have to be extremely accurate and then their control system is extremely complex. Recently, important researches in the nano-technologies have led to the development of new kind of solid-state switches [6] that fully satisfy the operating constrains and since those devices are part of the RF receivers for wireless comunication they are now large-scale products [7]. On the other hand, the increasing of the computational speed of the digital controllers, the miniturization of the devices, the decreasing of the costs of the digital equipment show that the technological gap to realize the time-modulated arrays have been overcame.

As a result, the synthesis of time-modulated (TM) arrays has received a renewed interest in recent years. The scientific community has focused its attention mainly on three frameworks: the extension the range of the applications of the time-modulation principles to other antenna synthesis problems, the review and formalization of the mathematical background of the time-modulated arrays and the development of innovative approaches to reduce the undesidered harmonic radiations (called sideband radiations SRs) that arise when the element excitations are modulated by means of sequence of time pulses.

More in detail, in order to properly address such issues and improving the efficiency of the approach with respect to the results in [3], suitable evolutionary optimization algorithms have been recently considered [8]-[13]. In [8] and [9], the sideband level (SBL) has been significantly reduced through the optimization of the "static-mode" coefficients as well as of the durations of the time pulses by

means of a Differential Evolution (DE) algorithm. A similar DE-based technique has been successively adopted in the synthesis of moving phase center antenna arrays for radar applications [10][11] to suppress the sideband radiations and to increase the passband of the receiver. Moreover, a Simulated Annealing (SA) technique has been used in [12] to minimize the sidelobe level (SLL) at the carrier frequency as well as the SBL of a time-modulated array with uniformly-excited elements. A different time schema has been successfully exploited in [13], where the modulation period has been quantized into shorter time steps and the on-off sequence optimized by means of a Genetic Algorithm (GA).

Concerning the applicability issues, a careful analysis has been carried out in [5] and [14], where suitable conditions for information transmission, and not only radar detection, have been formalized, as well. Additionally, some recent prototypes of time-modulated arrays exploiting different feeding schemes have been presented: in [15] a prototype of two-element time-modulated array is proposed to provide electronic null scanning whereas in [16] a four-element time-switched array system is used to find the direction of arrival of a signal feeding the elements with asymmetric switching waveforms. In [17] an analysis of phase-switched screens (PSS) based on time-switched array theory is introduced.

Although significant contributions in dealing with time modulation have been proposed, further investigations are needed in order to fully exploit the potentialities of the time-modulated arrays. In detail, this thesis is aimed at exploring the properties of time-modulated arrays by showing and discussing the results obtained when time is used as additional degrees of freedom in the synthesis process. More specifically, starting from the mathematical proof that the sideband radiations is a function of the "switch-on intervals" (i.e., the durations of the rectangular time pulses of the time modulation sequence), likewise the pattern shape at the fundamental frequency and the "switch-on instants" (i.e., the time instants when the RF switches commute from open to short circuit), the optimization of those parameters is profitably performed for pattern synthesis purposes. The reduction of the wasted power radiated by the undesired harmonics is performed throughout the minimization of a suitable cost function that measures the distance between the obtained and the desired side band level, SBL (the highest level of each h-th harmonic pattern with respect to the peak value radiated at the carrier frequency).

However, such an approach presents some disadvantages. First, it enforces an "indirect" SRs reduction and moreover, it needs the computation of the SBL at each harmonic frequency. Consequently, the minimization procedure is very high time-consuming and it is necessary to neglect some higher harmonics reducing the effectiveness of the approach to prevent the SRs. In order to overcome such drawbacks, an innovative approach based on a Particle Swarm Optimizer (PSO) [18] profitably exploits a closed-form relationship derived in [5] that quantifies the total wasted power in sideband radiations in linear time-modulated arrays. Moreover, following the guidelines in [5] a new closed-form expression that measures

the total wasted power in planar time-modulated arrays has been derived. As a matter of fact, such a result allows to deal with the synthesis of time-modulated planar arrays because it avoids the evaluation of the set of higher harmonic patterns that is extremely time-consuming when the number of elements of the array increases.

Finally, in the framework of exploiting time as additional degree of freedom in other antenna synthesis problem, this thesis proposed a new strategy aimed at using the time-modulation for the synthesis of difference pattern in sub-arrayed array monopulse antenna for search-and-track radar applications [19] . In such a device, it is necessary to radiate two different beams (namely sum and a difference pattern) on the same antenna aperture. As a matter of fact, the optimal solution of implementing two independent feed network is almost impracticable due to required cost, the architecture complexity and arising electromagnetic interferences. The most common way to solve such a problem consists in generating an optimal sum pattern and a sub-optimal difference pattern, the latter synthesized by applying the subarray technique [20]. Accordingly, the synthesis is aimed at optimizing prespecified subarray layouts by synthetizing subarray and radiating element weights. In order to apply the time-modulation in this problem, starting from a set of static excitations generating an optimal sum at the carrier frequency, a compromise difference beam is synthesized through a sub-arraying pattern matching procedure [21] aimed at optimizing the pulse durations at the input ports of the sub-arrays. Successively, the SRs at the harmonic frequency are minimized by performing a Particle Swarm Optimizer (PSO) to set the switch-on instants of the time sequence.

Chapter 2

Synthesis of Time-Modulated Linear Arrays

The approach presented in this chapter regards a strategy aimed at reducing the sideband radiations in time-modulated linear arrays through the shift of the pulses that compose the sequence modulating the array excitations. As a first step, a careful analysis of the features involved in higher harmonics generation is done. Following the guidelines emerged from such an analysis an indirect minimization of the sideband radiation is performed throughout the minimization of a suitable cost function that measures the distance between the obtained and the desired sideband level of the patterns radiated by the undesired harmonics. Since the non-convexity of the problem in hand, a global stochastic optimizer, namely Particle Swarm Optimizer, has been adopted to optimize the switch-on instants of the pulse sequences. Moreover, further investigations on the instantaneous behavior of the antenna during the time-modulation has been carried out.

2.1 Introduction

The synthesis of time-modulated arrays considers that the antenna elements are equipped with a set of radio-frequency (RF) switches used to enforce a time-modulation to the static array excitations [1]. This technique has been firstly taken into account to radiate average low and ultra-low sidelobe patterns [3] and successively for wireless communication purposes [4]. Recently, some studies have renewed the interest of such an approach applying the time-modulation to different antenna synthesis problems [8], [5], [17]. Moreover, since the pattern of a time-modulated array can be easily controlled properly modifying the pulse sequences, the time-modulation seems to be also a promising tool to operate in complex interference scenarios [22].

Despite the aforementioned positive features, the modulation of element excitations generates undesired harmonic radiations (the so-called sideband radiations) (SRs) which unavoidably affect the performances of the time-modulated arrays thus limiting their pratical applicability. In order to minimize the power losses due by the SRs, effective approaches based on evolutionary algorithm have been proposed [5][8][9][12][13]. However, further investigations are needed to show and to discuss the results obtained when time is used as additional degree of freedom in the antenna synthesis process. In detail, the behavior of the radiating system during the modulation and all the parameters involved in the sideband radiations generation have to be taken into account in order to develop effective strategies able to deal with the time-modulated arrays.

Accordingly with those purposes, this chapter is organized as follows. In Section 2.2 the theory of the time-modulated linear array is breafly summarized and some details about the dependance of the radiated patterns from the static excitations, the normalized pulse duration and the switch-on instants are given. Successively, the problem is mathematically formulated defining a suitable cost function aimed at quantifying the closeness of each solution to the desired one. In Section 2.3 the results of selected experiments are reported, showing the behavior of the antenna during the time modulation (Section 2.3.1). Moreover, the effectiveness of the proposed approach in dealing with the synthesis of time-modulated array is pointed out considering as parameters to optimize only the switch-on instants (Section 2.3.2) and both the switch-on instants and the normalized pulse duration (Section 2.3.3). Finally, in Section 2.4 some conclusions are pointed out.

2.2 Mathematical Formulation

Let us consider a time-modulated linear array ($TMLA$) composed by N identical elements equally-spaced of d along the z axis. The spatial distribution of the array elements is supposed to be symmetrical about the on-off sequences $U_n(t)$, $n = 0, \ldots, N-1$, which modulate the array element excitations, that are

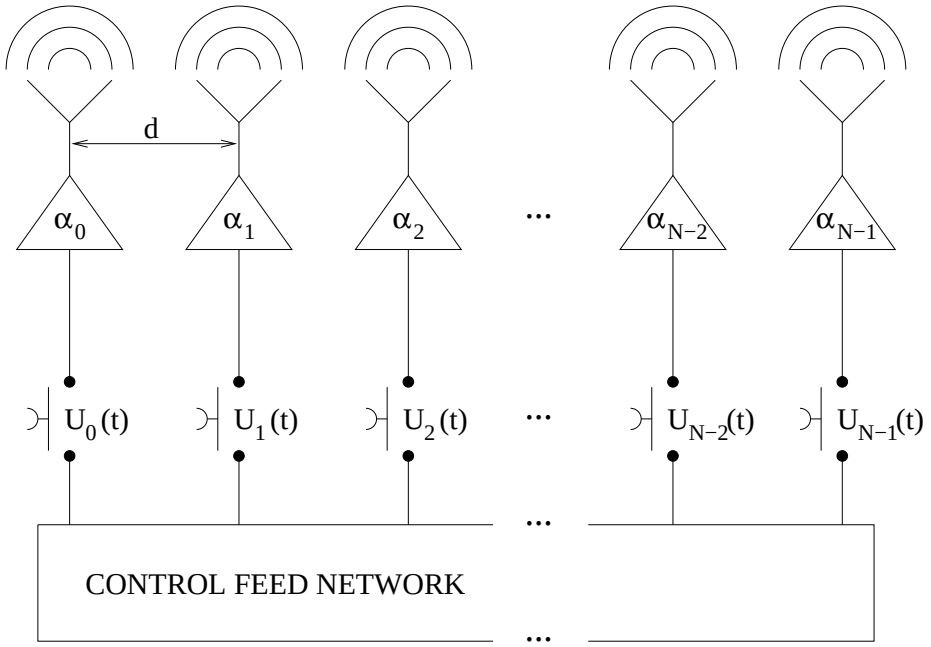

Figure 2.1: Sketch of the time-modulated linear array antenna.

obtained by means of on-off RF switches [Figure 2.1].

The arising far-field radiation pattern can be expressed as follows [3]:

$$F(\theta, t) = e_0(\theta)\, e^{j\omega_0 t} \sum_{n=0}^{N-1} \alpha_n U_n(t)\, e^{jkn\cos\theta} \tag{2.1}$$

where in (2.1), $e_0(\theta)$ and $\omega_0 = 2\pi f_0$ denote the element factor and the central angular frequency, respectively. Moreover, $k = \frac{2\pi}{\lambda}$ is the background wavenumber, $\mathbf{A} = \{\alpha_n,\, n = 0, \ldots, N-1\}$ is the set of static and complex array excitations, and θ indicates the angular position with respect to the array axis. The function $U_n(t)$ [Figure 2.2] is assumed to have a period equal to T_p and it is mathematically described as:

$$U_n(t) = \begin{cases} 1,\, t'_n \leq t \leq t''_n \\ 0,\, otherwise \end{cases} \tag{2.2}$$

where $0 \leq t'_n \leq t''_n \leq T_p$.
Moreover, the condition $T_p \gg T_0 = \frac{1}{f_0}$ is supposed to hold true [5]. Since $U_n(t)$ is a periodic function, it can be expressed in its Fourier representation as:

$$U_n(t) = \sum_{h=-\infty}^{+\infty} u_{hn} e^{jh\omega_p t} \tag{2.3}$$

being u_{hn} the $h-th$ Fourier coefficient, given by:

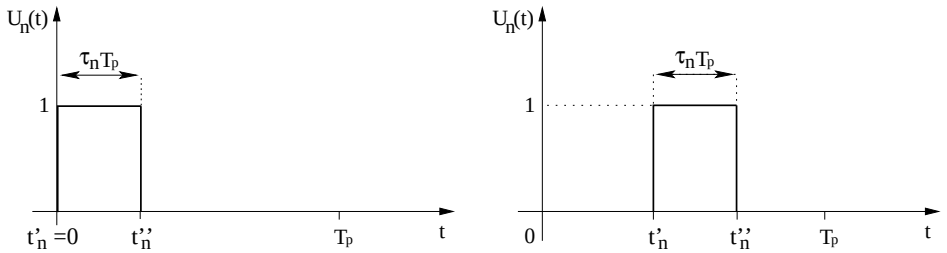

Figure 2.2: Time pulse when (a) $0 \leq \frac{t'_n}{T_p} \leq (1-\tau_n)$ and (b) $(1-\tau_n) \leq \frac{t'_n}{T_p} \leq 1$

$$u_{hn} = \frac{1}{T_p} \int_0^{T_p} U_n(t)\, e^{-jh\omega_p t} \tag{2.4}$$

being $\omega_p = 2\pi f_p = \frac{2\pi}{T_p}$ the fundamental angular frequency.
By considering isotropic radiators, [i.e., $e_0(\theta) = 1$] and without any loss of generality of the arising conclusions, the radiated far-field pattern turns out to be:

$$F(\theta, t) = \sum_{h=-\infty}^{+\infty} \left[\sum_{n=0}^{N-1} a_{hn} e^{jknd\cos\theta} \right] e^{j(h\omega_p + \omega_0)t} = \sum_{h=-\infty}^{+\infty} F_h(\theta, t) \tag{2.5}$$

where in equation (2.5) $a_{hn} = \alpha_n u_{hn}$; $n = 0, \ldots, N-1$. With reference to (2.5), the beam pattern at the carrier frequency f_0 depends on the $0-th$ order coefficients [3], [8], [12]:

$$a_{0n} = \alpha_n u_{0n},\ n = 0, \ldots,\ N-1 \tag{2.6}$$

where u_{0n} is the $0-th$ order Fourier coefficient [Equation 2.4 - $h = 0$] equal to:

$$u_{0n} = \frac{1}{T_p} \int_0^{T_p} U_n(t)\, dt = \tau_n \tag{2.7}$$

being $\tau_n = \frac{(t''_n - t'_n)}{T_P}$ the normalized $n-th$ time pulse duration. It is worth noticing [Equation (2.6)] that, when the values of the complex static excitations, α_n, $n = 1, \ldots, N-1$ are fixed, the pattern generated at the fundamental frequency ($h = 0$) is only function of the pulse duration τ_n, $n = 1, \ldots, N-1$. Accordingly, it is possible to synthetize a desired pattern, $\widehat{F}_0(\theta, t)$, different from the "static mode" (i. e., the mode generated by the static excitation set $\mathbf{A}$), by simply enforcing a suitable on-off time sequence to the static array excitations such that $\alpha_n \tau_n = \widehat{a}_{0n}$, $n = 0, \ldots, N-1$, (under the condition that $\arg(\alpha_n) = \arg(\widehat{a}_{0n})$

since τ_n, $n = 1, \ldots, N-1$ are real-valued quantities), $\widehat{a}_{0n}$ being the $n-th$ target excitation.
Unfortunately, the radiation patterns at the harmonic frequencies have significant components in the boresight direction [12]. In order to overcome such a drawback let us observe that the sideband radiation coefficients ($h \neq 0$):

$$a_{hn} = \frac{\alpha_n}{T_P}\left(\frac{e^{-jh\omega_p t'_n} - e^{-jh\omega_p t''_n}}{jh\omega_p}\right), n = 0, \ldots, N-1, \tag{2.8}$$

can be also expressed, after simple mathematical manipulations, as follows:

$$a_{hn} = \begin{cases} \alpha_n \tau_n sinc\left(\pi h \tau_n\right) e^{-j\pi h\left(\tau_n + 2\frac{t'_n}{T_p}\right)} & if\ 0 \leq \frac{t'_n}{T_p} \leq (1-\tau_n) \\ \frac{1}{\pi h}\left\{\sin\left[\pi h\left(1 - \frac{t'_n}{T_p}\right)\right] e^{-j\pi h\left(1+\frac{t'_n}{T_p}\right)} + \right. & \\ \left. \sin\left[\pi h\left(\frac{t'_n}{T_p} + \tau_n - 1\right)\right] e^{-j\pi h\left(\frac{t'_n}{T_p}+\tau_n-1\right)}\right\} & if\ (1-\tau_n) < \frac{t'_n}{T_p} \leq 1 \end{cases}. \tag{2.9}$$

Such an expression points out that the coefficients related to the undesired harmonic radiation depend on the pulse durations τ_n, $n = 0, \ldots, N-1$, analogously to the fundamental frequency counterparts [Equation (2.6)], but also on the switch-on time instants, t'_n, $n = 0, \ldots, N-1$. Thanks to this property, it is possible to spread the power associated to the SR as uniformly as possible over the whole visible angular space above the antenna (i.e., lowering the levels of the undesired harmonics along the boresight direction) by keeping the τ_n, $n = 0, \ldots, N-1$ values and optimizing the pulse shifts t'_n, $n = 1, \ldots, N$ [Figure 2.2].
Accordingly, a suitable strategy based on a Particle Swarm Optimizer (PSO) [18][23] is used to minimize the following cost function Ψ that quantifies the mismatch between the user-defined sideband level, SBL^{ref}, and the sideband levels, $SBL^{(h)} = SBL\left(\omega_0 + h\omega_p\right)$, $h = 1, ..., \infty$, of the synthesized pattern:

$$\Psi\left(\mathbf{t}'\right)|_{\mathbf{T}=\widehat{\mathbf{T}}} = \sum_{h=1}^{\infty}\left\{H\left[SBL^{ref} - SBL^{(h)}\left(\mathbf{t}'\right)\right]\left|\Delta_{SBL}^{(h)}\left(\mathbf{t}'\right)\right|^2\right\} \tag{2.10}$$

where in Equation (2.10) $\Delta_{SBL}^{(h)}\left(\mathbf{t}'\right) = \frac{SBL^{ref} - SBL^{(h)}(\mathbf{t}')}{SBL^{ref}}$, $\mathbf{t}' = \{t'_n;\ n = 0, ..., N-1\}$, $\mathbf{T} = \{\tau_n;\ n = 0, ..., N-1\}$, and $H(\cdot)$ stands for the Heaviside step function. On the other hand, when the constraint of exactly matching the desired pattern at f_0, $\widehat{F}_0\left(\theta, t\right)$, is relaxed [e.g., the synthesized pattern $F\left(\theta, t\right)$ is required at f_0 to fit the desired one in terms of SLL and main lobe beamwidth BW], it is still possible to profitably exploit the "pulse shifting" paradigm by tuning the pulse durations, τ_n, $n = 0, ..., N-1$, as well, to reduce the power losses of the

SR together with the corresponding SBL. Towards this end, the optimization is reformulated by defining the following matching function composed by three terms:

$$\begin{aligned}\Psi(\mathbf{t}', \mathbf{T}) &= \psi_{SLL}\left\{H\left[\Delta_{SLL}(\mathbf{T})\right]\left|\Delta_{SLL}(\mathbf{T})\right|^2\right\} + \\ &+\psi_{BW}\left\{H\left[\Delta_{BW}(\mathbf{T})\right]\left|\Delta_{BW}(\mathbf{T})\right|^2\right\} + \\ &+\psi_{SBL}\sum_{h=1}^{\infty}\left\{H\left[\Delta_{SBL}^{(h)}(\mathbf{t}', \mathbf{T})\right]\left|\Delta_{SBL}^{(h)}(\mathbf{t}', \mathbf{T})\right|^2\right\}\end{aligned} \tag{2.11}$$

where $\Delta_{SLL}(\mathbf{T}) = \frac{SLL^{ref} - SLL(\mathbf{T})}{SLL^{ref}}$ and $\Delta_{BW}(\mathbf{T}) = \frac{BW^{ref} - BW(\mathbf{T})}{BW^{ref}}$. Moreover, ψ_{SLL}, ψ_{BW}, ψ_{SBL} are real-valued weighting coefficients.

2.3 Numerical Validation

In order to assess the effectiveness of the proposed method, an exhaustive set of numerical experiments has been performed and some representative results will be shown in the following. More in detail, the discussion is firstly devoted to point out the behavior of the radiated pattern at the different instants within the modulating period T_p, whetever the pulse-shifting is present or not. In such a case, it is still possible to consider the classical pattern features (e.g., the maximum level of the secondary lobes, SLL, the main lobe beamwidth, BW, and the peak directivity, D_{max} [24]) for an heuristic analysis of the antenna performances. Successively, the efficiency of the proposed pulse-shift strategy in minimizing the SBL is illustrated. Toward this end and for comparative purposes, some illustrative test cases have been chosen among those already considered in the published literature. Moreover, the examples under analysis are concerned with both the SBL minimization and the SR power reduction.

2.3.1 Time-Modulated Radiated Pattern Behavior

In order to analyze the behavior of the radiated pattern at different instants of T_p let us consider an antenna array of $N = 16$ equally spaced of $d = \lambda/2$. The time-modulation is used to synthesize an average pattern equal to a Dolph-Chebyshev pattern with $SLL = -30\,[dB]$ at the central frequency ($h = 0$). According to the result reported in [25], the time pulses have been chosen to start coherently (i.e., $t'_n = 0$, $n = 0, \ldots, N-1$), and they have been set to the values $\tau_n = \tau_n^{DC}$, $n = 1, \ldots, N-1$, computed as in [26] and reported in Table 2.1, where for symmetry, only half-array is considered. The power losses due to the SRs [5] of such an arrangement amount to 24.2% of the total input power.

As regards to the antenna behavior in correspondence with fractions of the modulating period T_p, the directivity patterns radiated at $\frac{t}{T_p} = \{0.1, 0.4, 0.7, 1.0\}$ are shown in Figure 2.3, where the switch insertion loss present in actual feed

$N = 16$			$N = 30$		
n	τ_n^{DC}	$\frac{t_n'}{T_p}$	n	τ_n^{SA}	$\frac{t_n'}{T_p}$
8	1.000	0.256	1	0.065	0.599
9	0.953	0.740	3	0.076	0.461
10	0.864	0.661	4	0.072	0.583
11	0.744	0.426	5	0.065	0.815
12	0.603	0.594	6	0.880	0.514
13	0.458	0.300	23	0.965	0.823
14	0.319	0.629	27	0.171	0.580
15	0.295	0.978	28	0.473	0.000
–	–	–	29	0.976	0.812

Table 2.1: *Pattern Behavior* - Values of the switch-on times and switch-on instants optimized by means of the PS strategy.

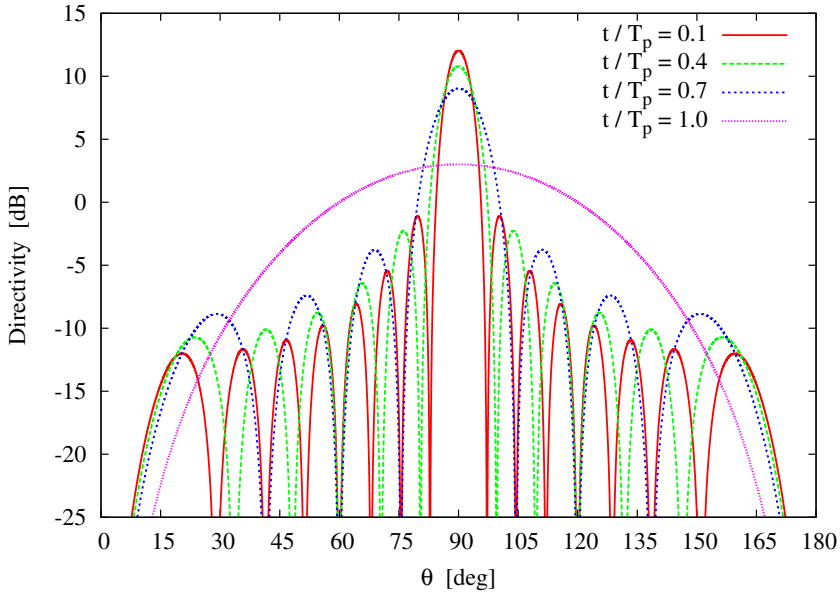

Figure 2.3: *Pattern Behavior* ($N = 16$, $d = 0.5\lambda$) - Plots of the directivity patterns obtained at the carrier frequency when sampling the current distribution on the array aperture at $\frac{t}{T_p} = \{0.1, 0.4, 0.7, 1.0\}$ for the DC solution.

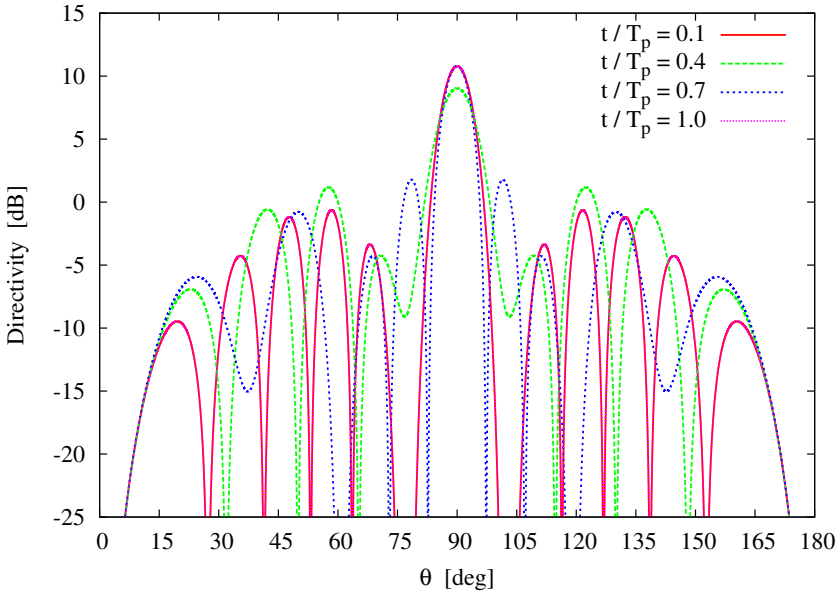

Figure 2.4: *Pattern Behavior* ($N = 16$, $d = 0.5\lambda$) - Plots of the directivity patterns obtained at the carrier frequency when sampling the current distribution on the array aperture at $\frac{t}{T_p} = \{0.1, 0.4, 0.7, 1.0\}$ for the solution obtained by means of PS technique.

networks is neglected. As expected, the instantaneous patterns differ from the Dolph-Chebyshev one and the antenna performances depend on the number of active elements at the sampling instant. With reference to Figure 2.3, it can be noticed that starting from $\frac{t}{T_p} = 0$, when all the array elements are turned on, the efficiency of the array gets lower and lower since the elements are successively switched off. Such a monotonically decreasing behavior can be avoided by optimizing the switch-on instants, t'_n, $n = 0, ..., N-1$, and keeping the pulse durations fixed to those of the Chebyshev distribution ($\tilde{\tau_n} = \tau_n^{DC}$, $n = 0, ..., N-1$). As far as the Particle Swarm (PS) procedure is concerned, a swarm of 10 particles have been used, and the control parameters have been set to $w = 0.4$ (intertial weight) and $C_1 = C_2 = 2$ (cognitive and social acceleration coefficients). The PS-optimized values of t'_n, $n = 0, ..., N-1$, are given in Table 2.1. Thanks to this operation, the number of switched-on elements at each instant of T_p is kept almost constant as well as the radiated patterns [Figure 2.4]. Such an event is further confirmed by the behavior of the pattern indexes in Figures 2.5 $(a)-(b)$ and related to D_{max}, SLL, and BW throughout the modulation period, respectively. For completeness, the statistics (minimum, maximum, mean values and variance) of the data in Figure 2.5 are reported in Table 2.2.

Although the maximum available directivity (i.e., $D_{max} = 12.04\,dB$) is never achieved when using the pulse-shifting approach, it is worth noticing that the

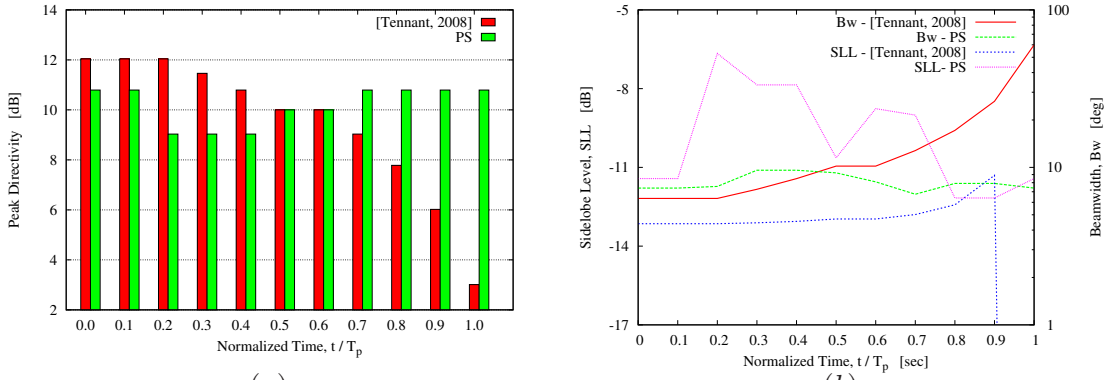

Figure 2.5: *Pattern Behavior* ($N = 16$ - $d = \lambda/2$) - Values of (a) D_{max} and of (b) SLL and BW for the DC solution and the solution obtained by means of the PS technique when sampling the current distribution on the array aperture at each tenth of the modulation period T_p.

Feature	$D_{max}\,[dB]$		$BW\,[deg]$		$SLL\,[dB]$	
Method	DC	PS	DC	PS	DC	PS
$min\{\cdot\}$	3.01	9.03	6.35	6.75	$-\infty$	-12.16
$max\{\cdot\}$	12.04	10.79	59.90	9.60	-11.30	-6.66
$av\{\cdot\}$	9.47	10.17	15.57	8.07	–	-9.80
$var\{\cdot\}$	7.53	0.59	229.31	0.86	–	3.63

Table 2.2: *Pattern Behavior* ($N = 16$, $d = 0.5\lambda$) - Statistics of the pattern indexes for the solutions without (DC) and with (PS) optimized switch-on instants.

mean value is greater than that of the original case ($av\{D_{max}\}^{PS} = 10.17\,dB$ vs. $av\{D_{max}\}^{DC} = 9.47\,dB$) and, more important, the directivity value is much more stable ($var\{D_{max}\}^{PS} = 0.59\,dB$ vs. $var\{D_{max}\}^{DC} = 7.53\,dB$). Differently, the DC solution starts at $t = 0.0$ from a maximum value of the directivity, $D_{max}\left(\frac{t}{T_p} = 0.0\right) = 12.04\,dB$, while only the two central elements are "on" at $t = T_p$ when the minimum value of directivity is obtained, $D_{max}\left(\frac{t}{T_p} = 1.0\right) = 3.01\,dB$. Similar conclusions arise from the analysis of the behavior of both the SLL and the BW [Figure 2.5(b) - Table 2.2]. It is worth pointing out that the mean value and variance of the SLL of the DC solution cannot be computed when $\frac{t}{T_p} = 1.0$ (i.e., $SLL = -\infty$) because of the absence of secondary lobes.

For completeness and in order to have some insights on the effects of mutual coupling (MC) interferences on the antenna aperture, the pattern obtained with

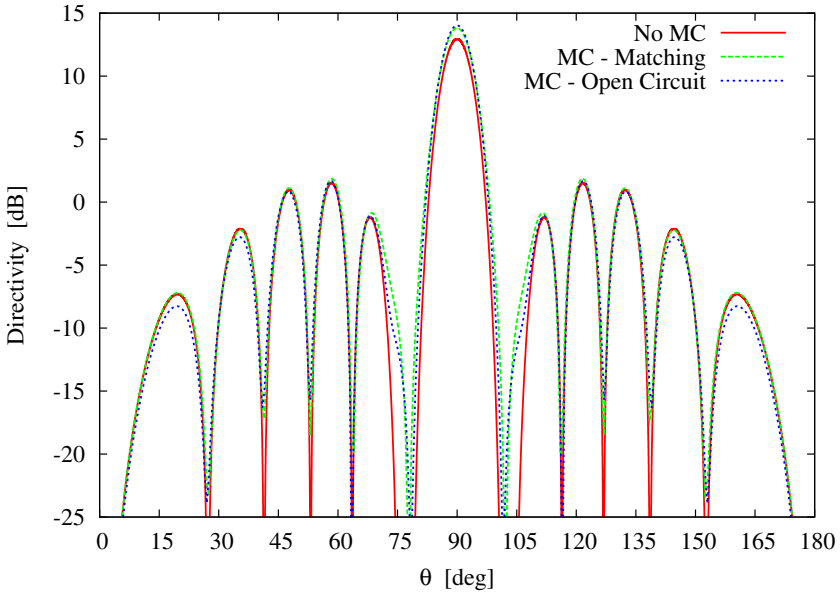

Figure 2.6: *Pattern Behavior* ($N = 16$, $d = 0.5\lambda$) - Directivity patterns obtained for a dipole array with and without mutual coupling at $\frac{t}{T_p} = 0.1$.

the PS configuration at $\frac{t}{T_p} = 0.1$ for an array of $\lambda/2$ dipoles of radius 0.002λ is reported in Figure 2.6 . The MC has been evaluated by considering two different impedance conditions (i.e., the perfect matching and the open circuit conditions) for the elements which are off. The mutual coupling does not seem to greatly effect the radiated pattern.

In the second experiment, the same synthesis problem dealt with in [12] by means of an approach based on Simulated Annealing (SA) has been considered. A uniform linear array of $N = 30$ elements spaced of $d = 0.7\lambda$ is considered where only 9 elements of the whole architecture are time-modulated. Analogously to the previous example, the durations of the time pulses have been set to those in [12] (i.e., $\tilde{\tau_n} = \tau_n^{SA}$, $n = 0, ..., N-1$) and given in Table 2.1. In this case, the percentage of power losses due to SRs is 3.9%. Once again, notwithstanding the reduced number of time-controlled elements, the plots in Figure 2.7 and the statistics in Table 2.3, assess that the optimization of the switch-on instants (Table 2.1) can be profitably exploited to keep the characteristics of the radiated pattern more stable during the modulation period T_p.

Feature	$D_{max}\,[dB]$		$BW\,[deg]$		$SLL\,[dB]$	
Method	*DC*	*PS*	*DC*	*PS*	*DC*	*PS*
$min\,\{\cdot\}$	13.42	13.62	3.38	3.56	-18.42	-18.42
$max\,\{\cdot\}$	14.77	14.31	3.98	3.98	-13.23	-14.87
$av\,\{\cdot\}$	13.91	13.94	3.82	3.79	-17.25	-17.09
$var\,\{\cdot\}$	0.11	0.03	0.03	$< 10^{-3}$	2.80	1.44

Table 2.3: *Pattern Behavior* ($N = 30$, $d = 0.7\lambda$) - Statistics of the pattern indexes for the solutions without (DC) and with (PS) optimized switch-on instants.

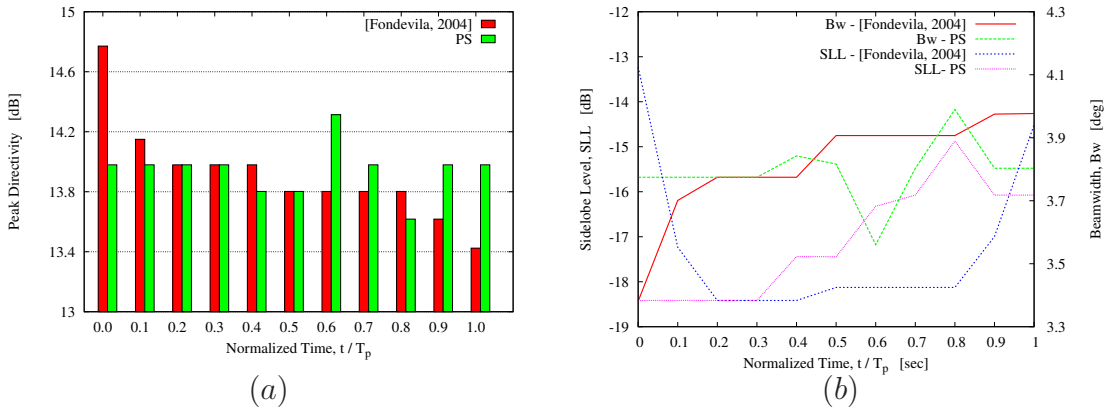

(*a*) (*b*)

Figure 2.7: *Pattern Behavior* ($N = 30$, $d = 0.7\lambda$) - Values of (a) D_{max} and of (b) SLL and BW for the DC solution and the solution obtained by means of the PS technique when sampling the current distribution on the array aperture at each tenth of the modulation period T_p.

2.3.2 SBL Reduction with Fixed Power Losses

In order to show the effectiveness of the proposed approach to reduce the sideband radiations, let us consider the same test cases presented in the previous section [12][25]. In detail, let us consider an array of $N = 16$ $\frac{\lambda}{2}$-spaced elements with the synthesis at the carrier frequency of a Chebyshev pattern with $SLL = -30\,[dB]$ [Figure 2.8 (a)] in which the set of the "static mode" excitations is uniform $\mathbf{A}^{(I)} = \{\alpha_n = 1;\, n = 0, \ldots, N-1\}$. Moreover, Figure 2.9 (a) gives a pictorial representation of the switching sequence synthetized in [25] by acting on $\mathbf{T}$. As expected [Equation (2.6)] the durations of the time pulses are equal to the values of the samples of the normalized Chebyshev distribution [26] (i.e., $\mathbf{T} = \mathbf{T}_{DC}$).
However, even though the reference pattern at f_0 is exactly matched, the harmonic content along the boresight direction is non-negligible [Figure 2.8(b)]. In order to cope with this drawback, the pulse-shifting technique has been then used as previously described. Accordingly, the set $\mathbf{t}'$ (being $\widehat{\mathbf{T}} = \mathbf{T}_{DC}$) has been optimized by choosing $SBL^{ref} = -25\,dB$ and minimizing the cost function in (2.10) with $h = 1$[1] since the power losses associated to higher harmonics decrease faster [5]. Towards this purpose, a PSO with $I = 10$ particles and a standard setting [27] of the control parameters (i.e., $w = 0.4$ and $C_1 = C_2 = 2$; w, C_1, and C_2 being the inertial weight and the cognitive/social acceleration terms, respectively) has been used.
The PSO-optimized pulse sequence is shown in Figure 2.9 (b). Moreover, the radiated patterns are displayed in Figure 2.10 and compared with those from [25] up to the second harmonic mode. As it can be observed, the SBL at $h = 1$ is equal to $SBL^{(1)}_{PSO} = -19.50\,dB$ and its value results more than $7\,dB$ below that in [25] (i.e., $SBL^{(1)}_{DC} = -12.40\,dB$).

Moreover, although the harmonic frequency $h = 2$ is not directly involved in the optimization process, it turns out that $SBL^{(2)}_{PSO} = -21.70\,dB$ vs. $SBL^{(2)}_{DC} = -18.30\,dB$. For completeness, the comparison in terms of maximum SBL of the harmonic patterns is extended to higher orders (Figure 2.11). It is worth noticing that over 30 harmonics, 29 PSO-synthesized patterns have SBLs lower than those generated by the pulse configuration $\mathbf{T}_{DC}$ in [Figure 2.8 (a)]. As a matter of fact, only the case $h = 16$ presents a SBL worse of almost $1\,dB$. Such a result further confirms the intrinsic "robustness" of the pulse shifting methodology. However, it should be remarked that the energy wasted in the SRs, which amounts to the 25.2% of the total input power [5], does not decrease through only pulse shifting. Moreover, since there is a trade-off (for a given antenna layout) between the possibility to arbitrary shape the pattern (i.e., desired SLL and beamwidth) at the carrier frequency and the presence of SR, the SBL could be higher than the SLL as shown in this case.
As far as the computational issues are concerned, the behavior of the optimal

[1] It should be pointed out that more terms (i.e., $h > 1$) might be considered in (2.10) to directly control the SBLs of other undesired harmonic terms.

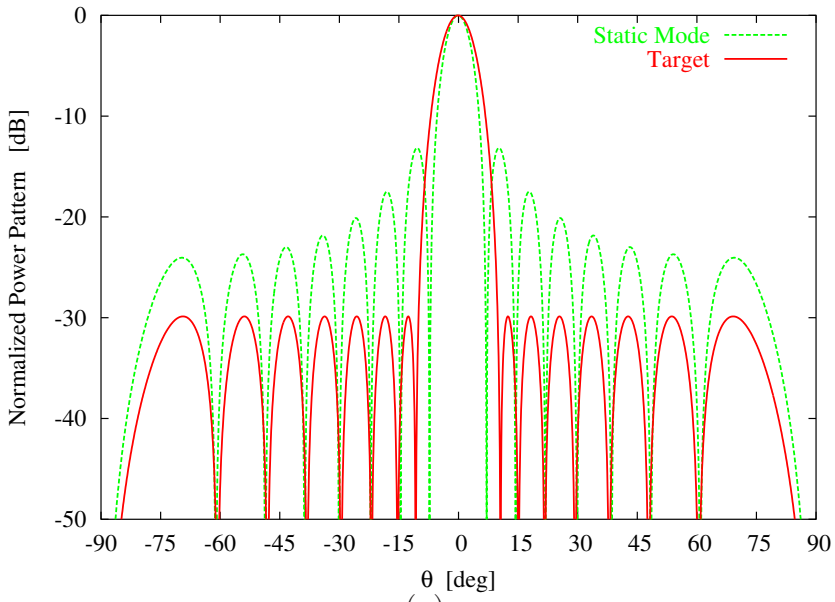

(a)

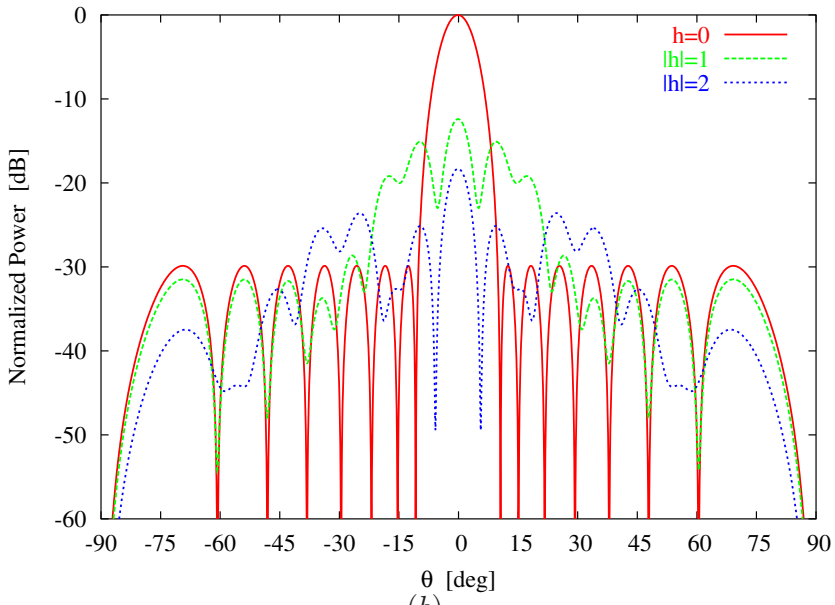

(b)

Figure 2.8: *Pulse Duration Optimization* [25] ($N = 16$, $d = 0.5\lambda$) - (a) Static and reference power patterns; (b) Power pattern generated at f_0 ($h = 0$) and in correspondence of the harmonic terms $h = 1, 2$.

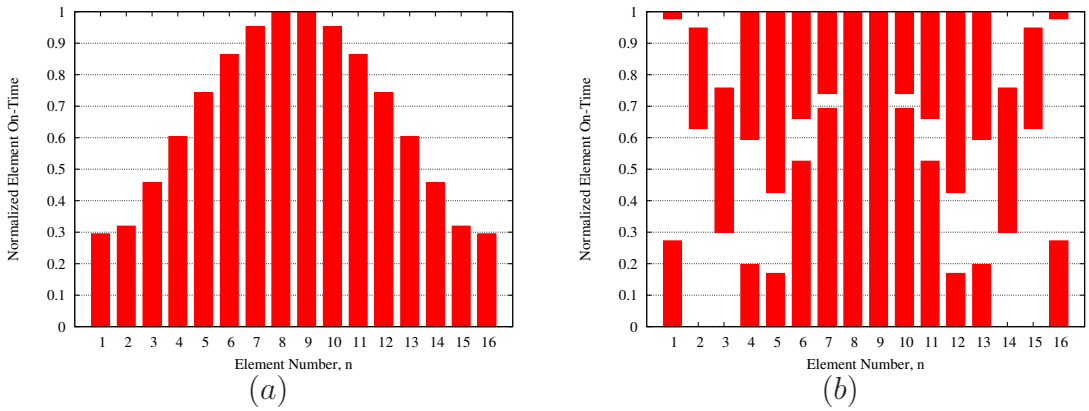

Figure 2.9: *Pulse Shift Optimization* ($N = 16$, $d = 0.5\lambda$) - Element on-off time sequence: (a) original [25] and (b) optimized with the *PSO*-based approach.

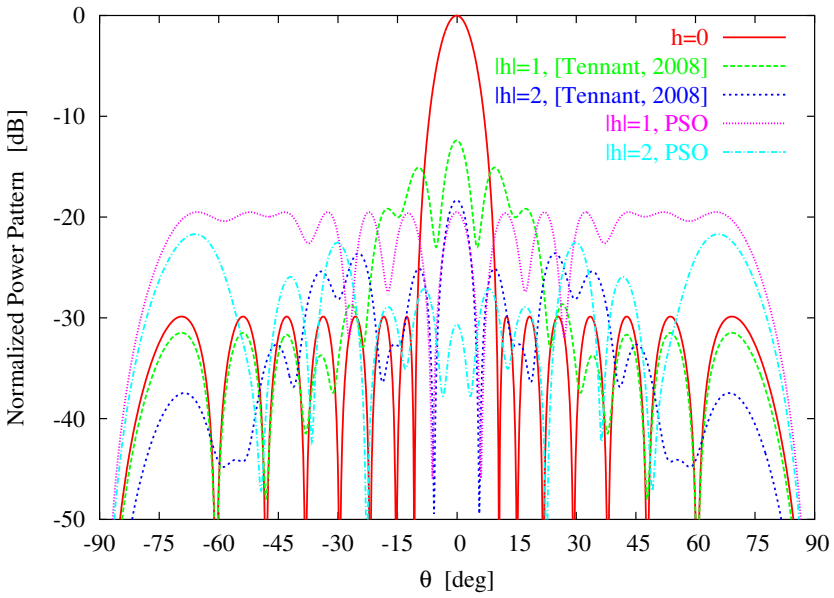

Figure 2.10: *Pulse Shift Optimization* ($N = 16$, $d = 0.5\lambda$) - Original [25] and *PSO*-optimized power patterns at $h = 0, 1, 2$.

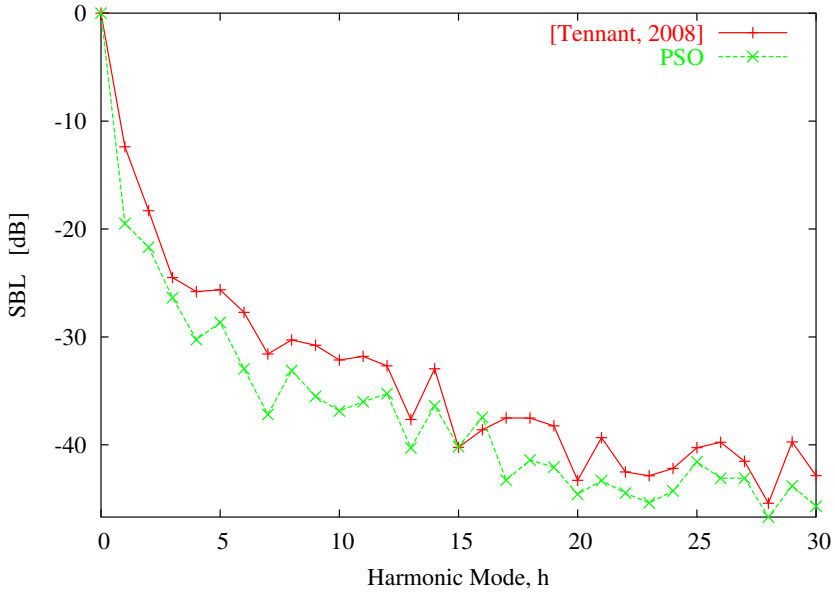

Figure 2.11: *Pulse Shift Optimization* ($N = 16$, $d = 0.5\lambda$) - Behavior of the $SBL^{(h)}$ when $h \in [0, 30]$. Original [25] and PSO optimized values.

value of Ψ (i.e., $\Psi^{opt} = min_k \left\{ min_i \left[\Psi \left(\mathbf{t'}_{i_k} \right)|_{\mathbf{T}=\mathbf{T}_{DC}} \right] \right\}$, i_k being the index of the i-th particle of the swarm at the k-th iteration of the minimization process) and the corresponding SBL values are reported in Figure 2.12. As regards to the CPU-time, it amounts to 74.16 $[sec]$ to complete the whole number of $K = 1000$ PSO iterations on a $3\,GHz$ PC with $1\,GB$ of RAM, 6.6×10^{-3} $[sec]$ being the time needed for a cost function evaluation.
The second experiment of this section refers to a scenario previously addressed in [12], where an array of $N = 30$ elements spaced by $d = 0.7\lambda$ has been considered. In [12], by exploiting a SA-based strategy, the set $\mathbf{T}$ has been optimized (i.e., $\mathbf{T} = \mathbf{T}_{SA}$) by minimizing a suitable cost function [Equation (5) - [12]] devoted to set the following constraints on the generated beam pattern: $SLL < -20\,dB$ and $SBL^{(h)} < -30\,dB$, $|h| = 1, 2$. Likewise the previous example, in order to prove that keeping the same time-duration set $\mathbf{T}_{SA}$ (i.e., the same pattern at $h = 0$), it is possible to further lower the SBL by properly programming the switch-on instants of the RF switches, the proposed PSO-based algorithm has been applied. The amount of power losses of the original configuration is equal to the 3.89%.
The original [12] and the PSO-optimized time sequence are reported in Figure 2.13 (a) and Figure 2.13 (b), respectively.
Moreover, Figure 2.14 shows the plots of the radiation patterns synthesized with the SA [12] and by means of the PSO algorithm at $|h| = 1$ and at the fundamental frequency ($h = 0$). As it can be observed, the level of the side-

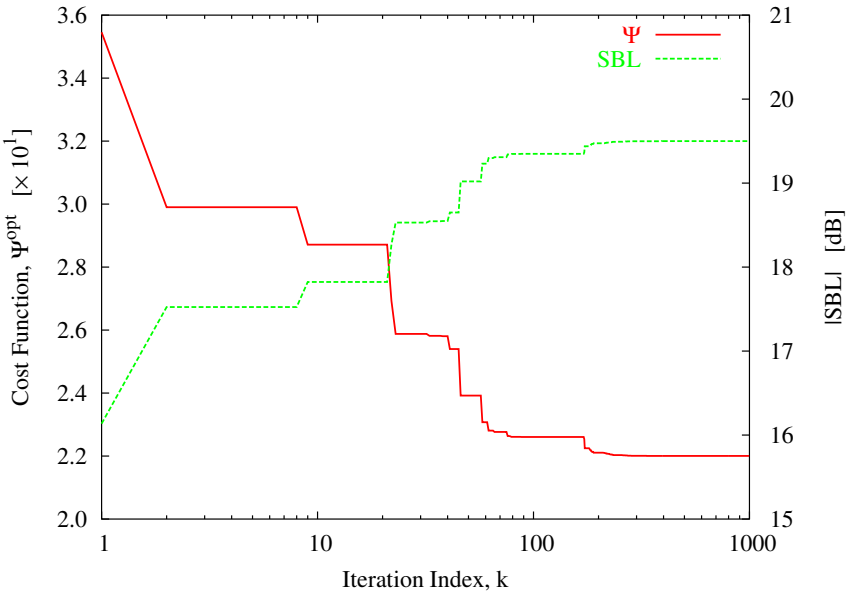

Figure 2.12: *Pulse Shift Optimization* ($N = 16$, $d = 0.5\lambda$) - Behaviors of the optimal value of the cost function, Ψ^{opt}, and of $SBL^{(1)}$ versus the iteration index k.

band radiation in correspondence with the first harmonic mode turns out to be $SBL^{(1)}_{SA} = -30.05\,dB$ while $SBL^{(1)}_{PSO} = -32.90\,dB$ with an improvement of about $3\,dB$ despite the reduced number of time modulated elements ($\frac{M}{N} < \frac{1}{3}$, $M = 9$ being the number of time-modulated elements). Furthermore, it is noteworthy that, thanks to the optimization of $\mathbf{t}'$, it also results $SBL^{(h)}_{PSO} < SBL^{(h)}_{SA}$, $h > 1$ [Figure 2.15].
For completeness, the behavior of Ψ^{opt} and the arising $SBL^{(1)}$ value versus the iteration index k are shown in Figure 2.16.

2.3.3 Joint SBL Minimization and SR Power Reduction

In order to assess the effectiveness of the pulse shifting technique also in dealing with the SR power reduction, let us consider the same benchmark of the first example in Sect. 2.3.1, but now optimizing the pulse durations, as well. Towards this aim, the cost function (2.11) is adopted and the reference thresholds are set to $SLL^{ref} = -30\,dB$ and $BW^{ref} = 3.95^o$ to obtain a pattern with the same features of that afforded by the Chebyshev coefficients, by keeping $SBL^{ref} = -25\,dB$. Figure 2.17 shows the pulse sequence synthesized by the PSO-based method when a swarm of $I = 20$ particles has been run for $K = 1000$ iterations.
As regards to the computational costs, the computational burden grows since the number of unknowns double with respect to the case in Sect. 2.3.2 and the

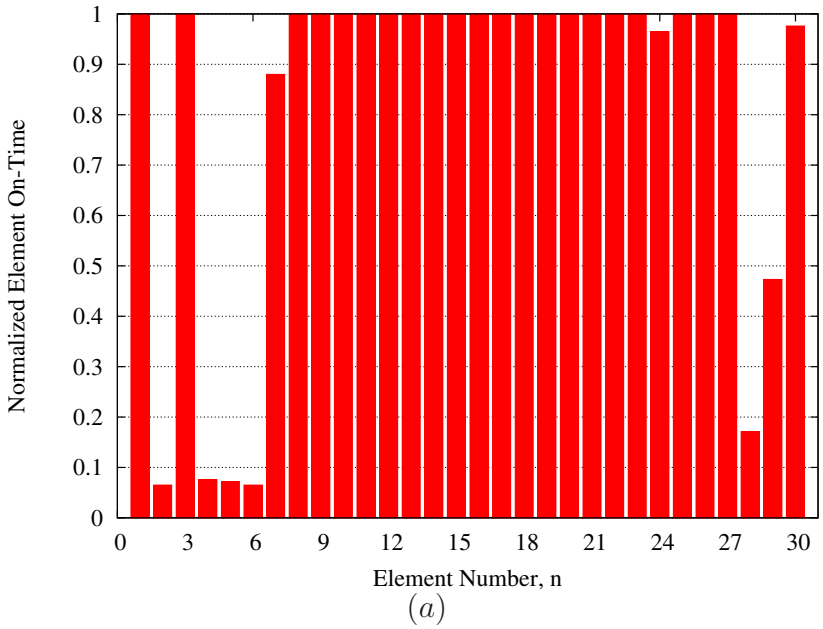

(a)

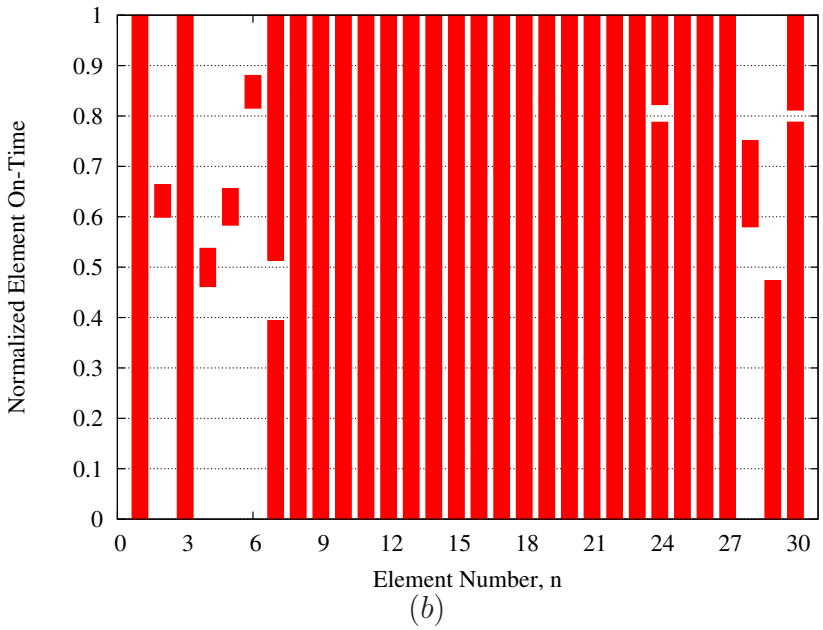

(b)

Figure 2.13: *Pulse Shift Optimization* ($N = 30$, $d = 0.7\lambda$) - Element on-off time sequence: (a) original [12] and (b) optimized with the PSO-based approach.

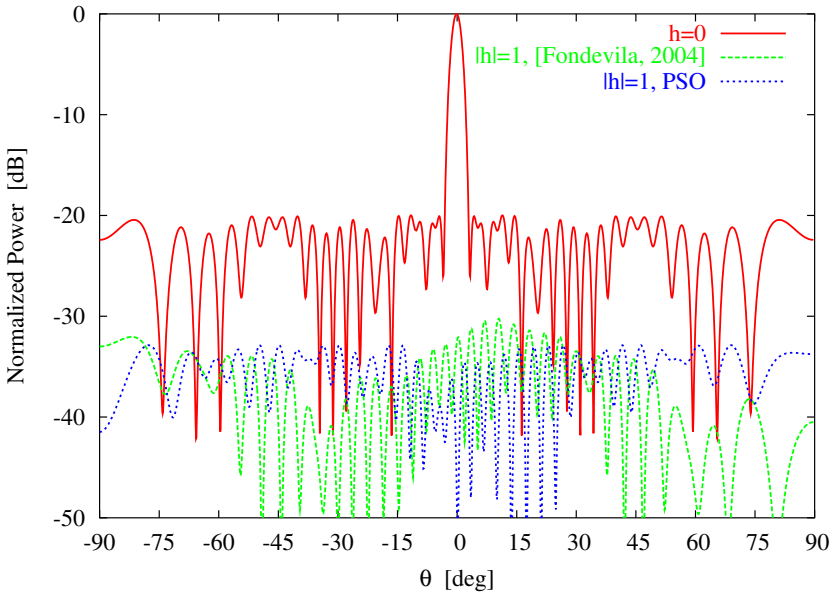

Figure 2.14: *Pulse Shift Optimization* ($N = 30$, $d = 0.7\lambda$) - Power patterns at f_0 ($h = 0$) and when $h = 1$: original [12] and PSO-optimized plots.

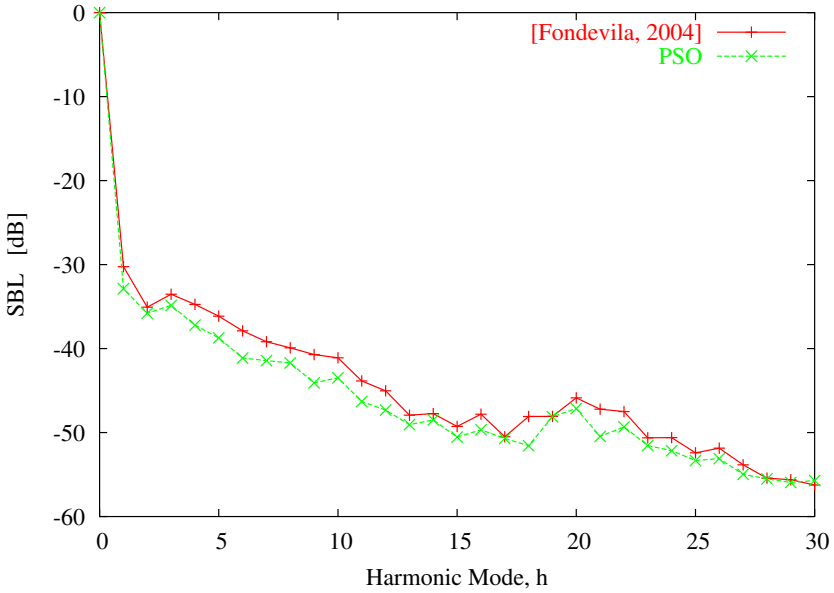

Figure 2.15: *Pulse Shift Optimization* ($N = 30$, $d = 0.7\lambda$) - Behavior of the $SBL^{(h)}$ when $h \in [0, 30]$. Original [12] and PSO optimized values.

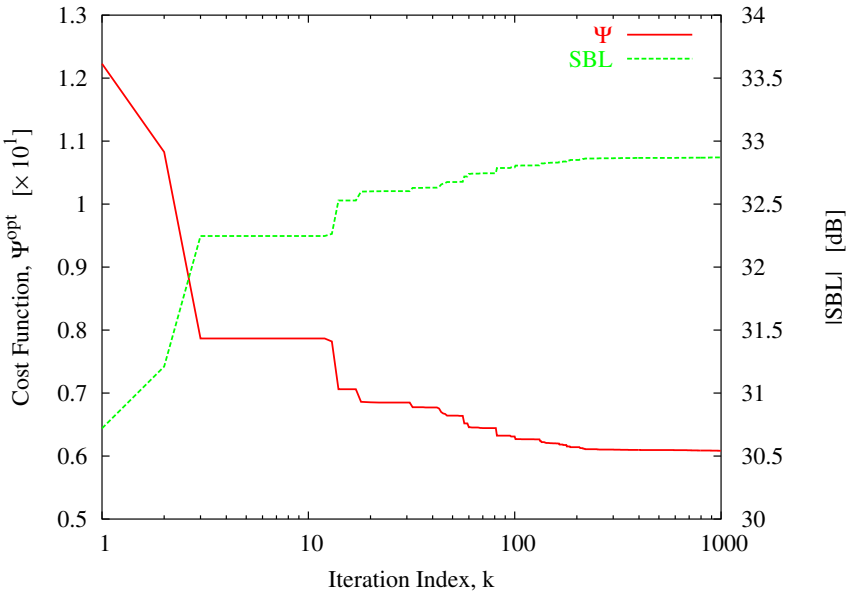

Figure 2.16: *Pulse Shift Optimization* ($N = 30$, $d = 0.7\lambda$) - Behaviors of the optimal value of the cost function, Ψ^{opt}, and of $SBL^{(1)}$ versus the iteration index k.

solution space of the admissible solutions significantly enlarges.

For comparison purposes, the normalized powers related to f_0 and to the sideband radiations are analyzed and Figure 2.18 shows the results obtained when acting on $\mathbf{T}$ [25] and also on $\mathbf{t}'$. As expected, there is a reduction of the losses due to the SR and an increasing of the radiation at f_0 when applying the pulse shifting. It is worthwhile to point out that such an enhancement of the performance is yielded without increasing the architectural complexity of the system with uniform excitations. For completeness, the patterns synthesized at the carrier frequency and when $h = 1, 2$ are shown in Fig. 2.19 and compared with those from the time-modulation scheme in Figure 2.9 (a). Moreover, the CPU-time necessary to compute the cost function value (2.11) of each particle is about twice that when only $\mathbf{t}'$ was optimized (2.3.2). Consequently, the total CPU-time required to sample the solution space with a swarm of $I = 20$ particles amounts to 262.01 $[sec]$, 1.3×10^{-2} $[sec]$ being the time-cost of a single evaluation of $\Psi(\mathbf{t}', \mathbf{T})$.

Finally, Figure 2.20 gives some indications on the behaviors of the three terms of the cost function as well as of Ψ^{opt} throughout the iterative optimization process.

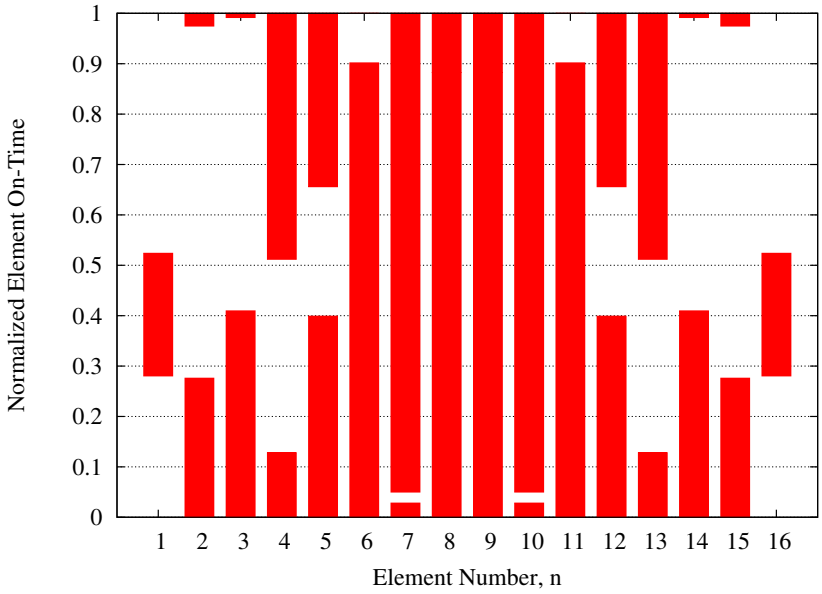

Figure 2.17: *Joint Optimization of Pulse Shifts and Durations* ($N = 16$, $d = 0.5\lambda$) - *PSO*-optimized element on-time sequence.

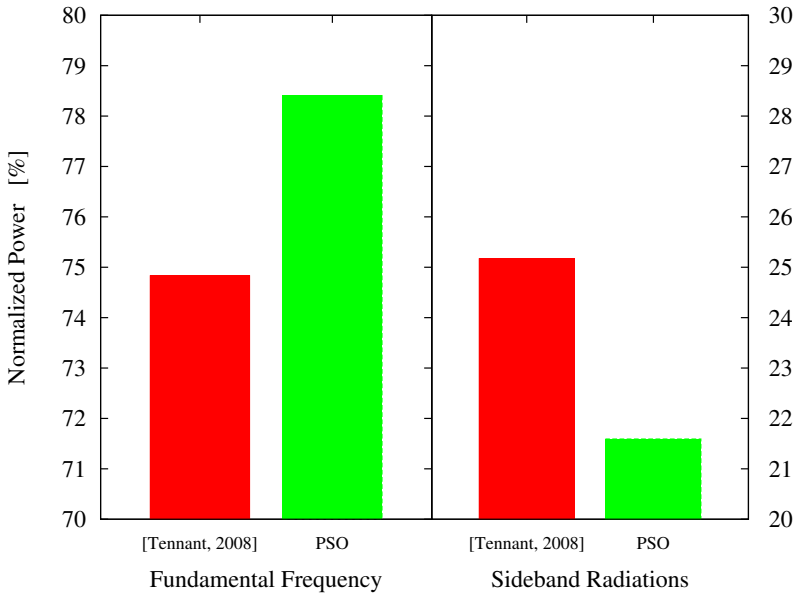

Figure 2.18: *Joint Optimization of Pulse Shifts and Durations* ($N = 16$, $d = 0.5\lambda$) - Normalized powers associated to f_0 ($h = 0$) and to the sideband radiations ($h \neq 0$) for pulse duration optimization [25] and *PSO*-based shift-duration pulse optimization.

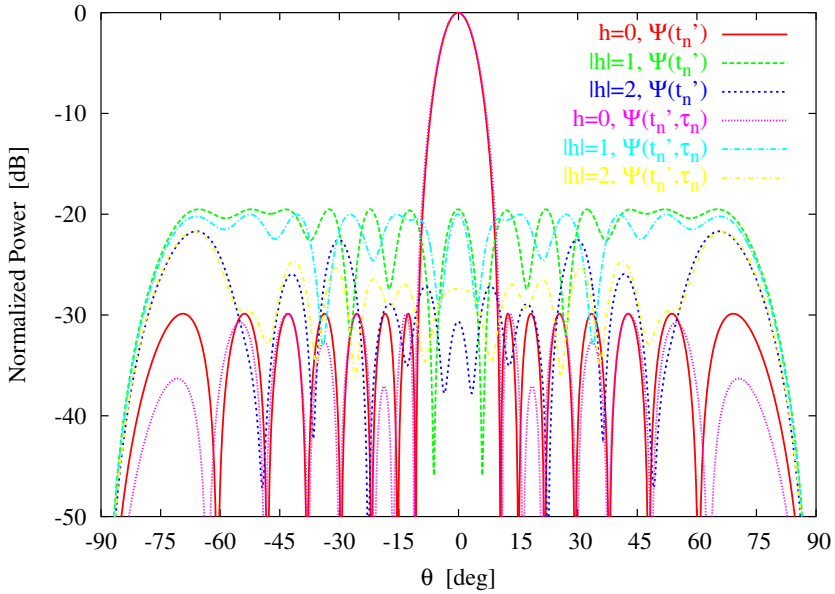

Figure 2.19: *Joint Optimization of Pulse Shifts and Durations* ($N = 16$, $d = 0.5\lambda$) - Normalized powers associated to f_0 ($h = 0$) and to the sideband radiations ($h \neq 0$) for pulse duration optimization [25] and *PSO*-based shift-duration pulse optimization.

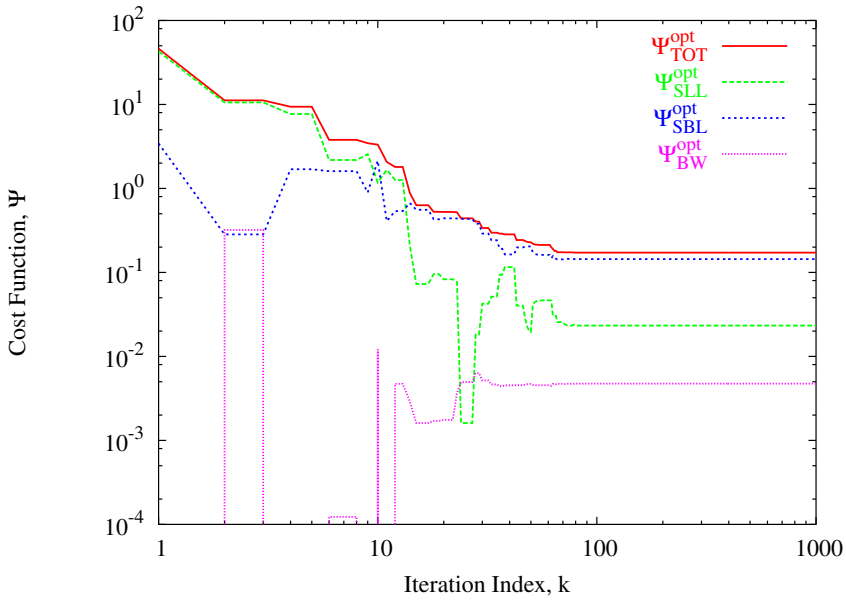

Figure 2.20: *Joint Optimization of Pulse Shifts and Durations* ($N = 16$, $d = 0.5\lambda$) - Behaviors of the cost function terms during the iterative *PSO*-based minimization

2.4 Discussions

In this chapter an innovative approach for the synthesis of time-modulated linear arrays has been proposed. The method considers the on instants of the time pulses as a suitable and further degree of freedom in the synthesis process. Starting from the basic principles of the pulse shifting strategy, mathematically formulated according to the theory of time-modulated arrays, the synthesis problem has been recast as the optimization of a proper cost function modelling the mismatch between the actual pattern features and the desired ones. Both $SBLs$ reduction and SRs minimization issues have been addressed and the minimization of the corresponding cost function has been carried out by means of a PSO-based algorithm. A set of representative results has been reported and discussed in order to assess the potentialities of the proposed approach. The pulse-shift methodology has demonstrated to work effectively when compared to other techniques in dealing with examples usually considered in the state-of-the-art literature.

Chapter 3

Direct Minimization of Sideband Radiations in Linear Time-Modulated Arrays

The approach presented in this chapter regards an enhanced strategy aimed at reducing the sideband radiations in time-modulated linear arrays. More in detail, a closed-form relationship that computes the power radiated by the undesired harmonics is profitably exploited in an optimization strategy based on the Particle Swarm Optimizer. Such an approach optimizes the switch-on instants of the pulse-sequence and allows a considerable saving of the computational burden.

3.1 Introduction

As pointed out in chapter 2, even if the time-modulated arrays can be profitably exploited to radiate low and ultra-low sidelobe patterns and their patterns can be easily controlled modifying the time sequences the generation of the undesired harmonics leads to an important waste of power (the sideband radiations SRs). Such a fact is the main drawback that has limited the use of such kind of antennas array in practical applications.

Recently, in order to reduce sideband radiations, different stochastic iterative algorithms have been proposed [8][9][12][13]. They are based on the minimization of the sideband levels ($SBLs$) at the higher order harmonics. However, such a guidelines presents some disadvantages. First, it enforces an "indirect" SRs reduction (i.e., through $SBLs$ minimization). Moreover, it needs the computation of the SBL at each harmonic frequency. As a matter of fact, neglecting some higher harmonics and considering just low orders could prevent a suitable SRs reduction.

In order to overcome these drawbacks, an innovative approach is proposed. It is based on a Particle Swarm Optimizer (PSO) aimed at synthesizing a desidered pattern with prescribed sidelobe level (SLL) at the carrier frequency also directly minimizing the power losses due to SRs. Toward this end, the closed-form relationship, derived in [5] to quantify the total power wasted in sideband radiations, is profitably exploited because its analytic form, its simplicity, and to avoid the evaluation of the (infinite) set of higher harmonic patterns.

Accordingly, the outline of this chapter is the following. In Section 3.2 the problem is mathematically formulated, summarizing the key-issues concerned with the time-modulation for the array synthesis. Successively, the PSO-based strategy to reduce the power losses due to SRs is presented. Moreover, in Section 3.3 a set of numerical results are reported and compared with other state-of-art solutions to point out the effectiveness of the approach. Finally, some conclusions are drawn (Section 3.4).

3.2 Mathematical Formulation

Let us consider a time-modulated linear array of N isotropic elements equally-spaced of d along the z axis. The elements are modulated by means of on-off RF switches controlled by on-off periodic pulses of period T_p, $U_n(t)$; $n = 0, \ldots, N-1$ (2.2). Following the procedure described in Section 2.2, the array factor appears to be the summation of an infinite number of harmonic contributions:

$$F(\theta, t) = \sum_{h=-\infty}^{+\infty} \left[\sum_{n=0}^{N-1} a_{hn} e^{jknd\cos\theta} \right] e^{j(h\omega_p + \omega_0)t} = \sum_{h=-\infty}^{+\infty} F_h(\theta, t) \qquad (3.1)$$

where in Equation (3.1), $k = \frac{2\pi}{\lambda}$ is the background wave-number, $\omega_0 = 2\pi f_0$ de-

notes the central angular frequency, θ indicates the angular position with respect to the array axis. Moreover, the coefficients a_{hn}; $n = 1, \ldots, N$ are computed as:

$$a_{hn} = \alpha_n \frac{1}{T_p} \int_0^{T_p} U_n(t)\, e^{-jh\omega_p t} dt \tag{3.2}$$

being $\underline{A} = \{\alpha_n;\, n = 0, \ldots, N-1\}$ the set of the static excitations of the array, $\omega_p = \frac{2\pi}{T_p}$ is the angular frequency of the modulating pulses. From Equation (3.1) follows that the central frequency beam ($h = 0$) is given by:

$$F^{(0)}(\theta, t) = e^{j\omega_0 t} \sum_{n=0}^{N-1} a_{0n} e^{jnd\cos\theta}, \tag{3.3}$$

while the sideband radiations turn out to be:

$$F_{SR}(\theta, t) = \sum_{h=\infty}^{+\infty} F^{(h)}(\theta, t) \tag{3.4}$$

being $F^{(h)}(\theta, t) = \left[\sum_{n=0}^{N-1} a_{hn} e^{jnd\cos\theta}\right] e^{j(h\omega_p + \omega_0)t}$. As far as the power losses due to the sideband radiations, they can be analytically quantified according to the following closed form [5]:

$$\begin{aligned} \mathcal{P}^{SR}(\underline{A}, \underline{\tau}) \;=\; & \sum_{n=0}^{N-1} \left\{ |\alpha_n|^2 \tau_n (1 - \tau_n) \right\} + \\ & \sum_{\substack{m,n=0 \\ m \neq 0}}^{N-1} \left\{ \Re\{\alpha_m \alpha_n^*\} \operatorname{sinc}[k(z_m - z_n)] (\tau_{mn} - \tau_m \tau_n) \right\} \end{aligned} \tag{3.5}$$

where in (3.5) $\Re\{\cdot\}$ and the apex * indicate the mean real part and complex conjugation, respectively. Moreover, $z_m = m \times d$ and $z_n = n \times d$ are the positions of the m-th and n-th array element along the z-axis, $\underline{\tau} = \{\tau_n;\, n = 0, ..., N-1\}$ is the set of normalized switch-on times whose n-th element is defined as $\tau_n = \frac{t_n}{T_p}$, while

$$\tau_{mn} = \begin{cases} \tau_n & if\ \tau_n \leq \tau_m \\ \tau_m & otherwise \end{cases}. \tag{3.6}$$

Therefore, it turns out that the SR power losses can be minimized by properly setting the values of the static excitations, $\underline{A}$, as well as the durations of the time pulses, $\underline{\tau}$. However, since we are interested in synthesizing antennas with a low number of control parameters, uniform and isophoric excitations (i.e., $\alpha_n = 1$, $n = 0, ..., N-1$) are assumed. Only the durations of the switch-on times are

then optimized by means of an iterative (k being the iteration index) PSO-based strategy aimed at minimizing the following cost function:

$$\Psi\left(\underline{\tau}\right) = w_{SLL}\Psi^{SLL}\left(\underline{\tau}\right) + w_P\mathcal{P}_k^{SR}. \tag{3.7}$$

The first term in (3.7), $\Psi^{SLL} = H\left[SLL^{ref} - SLL_k\right]\frac{\left|SLL^{ref}-SLL_k\right|^2}{\left|SLL^{ref}\right|^2}$, models a constraint on the array pattern at ω_0 and quantifies the distance between the current , SLL_k, and the desired sidelobe level, SLL^{ref}, while the latter is related to the power losses. Moreover, w_{SLL} and w_P are real weight coefficients and $H(\cdot)$ is the Heaviside step function.
As regards to the PSO-based minimization, the algorithm starts from randomly chosen guess values and updates at each iteration the set of S trial solutions, $\underline{\tau}_k^{(s)}$, $s = 1, ..., S$, as well as the corresponding PSO velocities, $\underline{v}_k^{(s)}$, $s = 1, ..., S$, as follows [18]:

$$\underline{v}_k^{(s)} = e\underline{v}_{k-1}^{(s)} + C_1 r_1\left(\underline{p}_k^{(s)} - \underline{\tau}_{k-1}^{(s)}\right) + C_2 r_2\left(\underline{g}_k - \underline{\tau}_{k-1}^{(s)}\right) \tag{3.8}$$

$$\underline{\tau}_k^{(s)} = \underline{\tau}_{k-1}^{(s)} + \underline{v}_k^{(s)}, \qquad s = 1, ..., S \tag{3.9}$$

where e (*inertial weight*), C_1 (*cognitive acceleration*), and C_2 (*social acceleration*) are the PSO control parameters. Moreover, r_1 and r_2 are two random variables having uniform distribution in the range $[0 : 1]$. Furthermore, $\underline{p}_k^{(s)} = \arg\left\{min_{q=1,...,k}\left[\Psi\left(\underline{\tau}_q^{(s)}\right)\right]\right\}$ and $\underline{\tau}_k^{opt} = \arg\left\{min_{s=1,...,S}\left[\Psi\left(\underline{p}_k^{(s)}\right)\right]\right\}$ are the so-called *personal best* solution and *global best* solution, respectively. The process is iterated until a convergence criterion based either on a maximum number of iterations K or the following stationary condition:

$$\frac{\left|K_{window}\Psi\left(\underline{\tau}_k^{opt}\right) - \sum_{q=1}^{K_{window}}\Psi\left(\underline{\tau}_{k-q}^{opt}\right)\Psi_l^{opt}\right|}{\Psi\left(\underline{\tau}_k^{opt}\right)} \leq \xi \tag{3.10}$$

holds true. In (3.10), K_{window} and ξ are a fixed number of iterations and a user-defined numerical threshold, respectively.

3.3 Numerical Validation

In order to give some indications on the effectiveness of the proposed approach in minimizing the power losses associated to the SRs, while synthesizing a fixed SLL pattern at the carrier frequency. Towards this purpose, some representative examples are reported and discussed also in a comparative fashion. Comments on the relationship between SRs minimization, performance (i.e., SLL) and complexity of the synthesized array are given, as well.

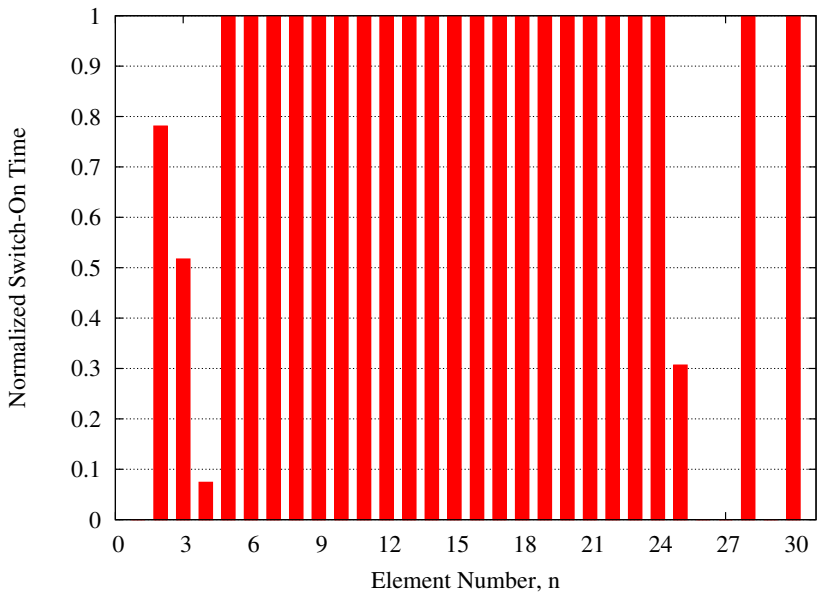

Figure 3.1: *SRs Minimization* ($N = 30$, $d = 0.7\lambda$) - Switch-on time sequence synthesized with the PSO-based approach.

Let us consider a linear array of $N = 30$ elements equally-spaced by $d = 0.7\lambda$. The same experiment has been previously dealt with in [12] with the aim of minimizing the sideband levels (SBLs) at $h = 1, 2$, while keeping a desired SLL at $\omega = \omega_0$. In [12], the optimization has been carried out by means of a Simulated Annealing (SA) approach by setting $SLL^{ref} = -20\,dB$ and $SBL^{ref} = -30\,dB$, respectively. The synthesized solution [12] fulfills both requirements (i.e., $SLL_{SA} = -20\,dB$, $SBL^{(1)}_{SA} = -30.2\,dB$, and $SBL^{(2)}_{SA} = -35.1\,dB$) by time-modulating only 9 elements over 30 and the power wasted in the sidelobe radiations amounts to $\mathcal{P}^{SR}_{SA} = 3.89$ % of the total input power. The directivity and the feed-network efficiency computed through the relationships in [28] are equal to $D^{T}_{SA} = 15.14\,dB$ and $\eta^{f}_{SA} = 0.82$, respectively.

As far as the PSO-based method is concerned, a swarm of $S = 10$ particles (i.e., trial solutions) has been chosen and the control parameters have been set to $w = 0.4$, $C_1 = C_2 = 2.0$, and $K = 1000$. Moreover, a uniform weighting has been assumed in (3.7) (i.e., $w_{SLL} = w_P = 1.0$). The numerical simulations have been run on a $3\,GHz$ PC with $1\,GB$ of RAM and the convergence has been reached after $K_{end} = 761$ iterations with a total and average (per iteration) CPU time equal $113.39\,[sec]$ and $0.149\,[sec]$, respectively. The time sequence synthesized at $k = K_{end}$ is shown in Figure 3.1 while the patterns afforded at the carrier frequency [Eq. (3.3)] and the first two harmonic patterns [Eq. (3.4) - $h = 1, 2$] are shown in Figure 3.2. As it can be noticed (Figure 3.2), only 4 elements are time modulated (vs. 9 in [12]) and the same performances of the SA-based

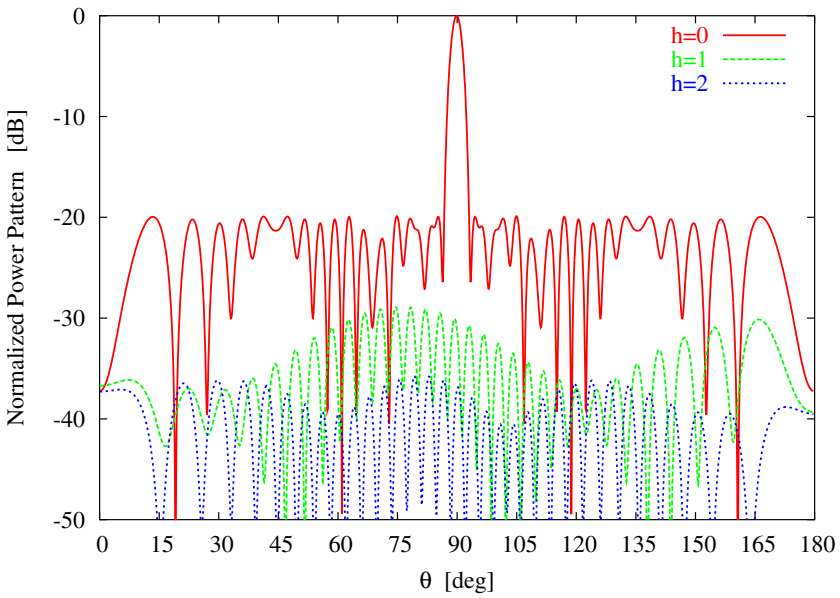

Figure 3.2: *SRs Minimization* ($N = 30$, $d = 0.7\lambda$) - Normalized power patterns at the carrier frequency ($h = 0$) and related to the sideband radiations ($h = 1, 2$) in correspondence with the pulse sequence in Figure 3.1.

approach have been obtained neglecting the elements 1, 26, 27, and 29, which are always turned off.

As regards to the fulfillment of the synthesis constraints, Figure 3.3 shows the behavior of $\Psi_k^{opt} = \Psi\left(\underline{\tau}_k^{opt}\right)$ and the values of the two terms in (3.7). As expected, the PSO solution widely fulfils the user constraint on the SLL at the convergence [i.e., $\Psi^{SLL}\left(K_{end}\right) < 10^{-6}$], when the stationary condition on the value of the cost function is reached. Concerning the SRs, although the sideband level of the first harmonic term of the PSO solution is higher than that synthesized with the SA approach (i.e., $SBL_{PSO}^{(1)} = -28.9\,dB$ vs. $SBL_{SA}^{(1)} = -30.2\,dB$ - Figure 3.4), the amount of power losses in the SRs turns out to be lower since $\mathcal{P}_{PSO}^{SR} = 3.57$ %. Such a result points out that a suitable strategy based on the direct minimization of the SRs, instead of the optimization of the SBLs [13][8][9][12], seems to be more effective in reducing power losses. On the other hand, it should be noticed that the proposed techniques also guarantees satisfactory SBLs since, besides the first harmonic ($h = 1$), $SBL_{PSO}^{(h)} < SBL_{SA}^{(h)}$ for $h \geq 2$. As a matter of fact, the reduction of the SBL ranges from a minimum of $\Delta_{min}^{SBL} = 0.7\,dB$ to a maximum equal to $\Delta_{max}^{SBL} = 11.5\,dB$, with an average value of around $\Delta_{av}^{SBL} = 6.2\,dB$. Conversely, the directivity as well as the feed-network efficiency slightly reduce to $D_{PSO}^{T} = 14.94\,dB$ and $\eta_{PSO}^{f} = 0.79$.

Finally, Figure 3.5 shows an analysis on the available compromises between antenna performance (i.e., directivity and SLL) and associated power losses, $\mathcal{P}^{SR}$,

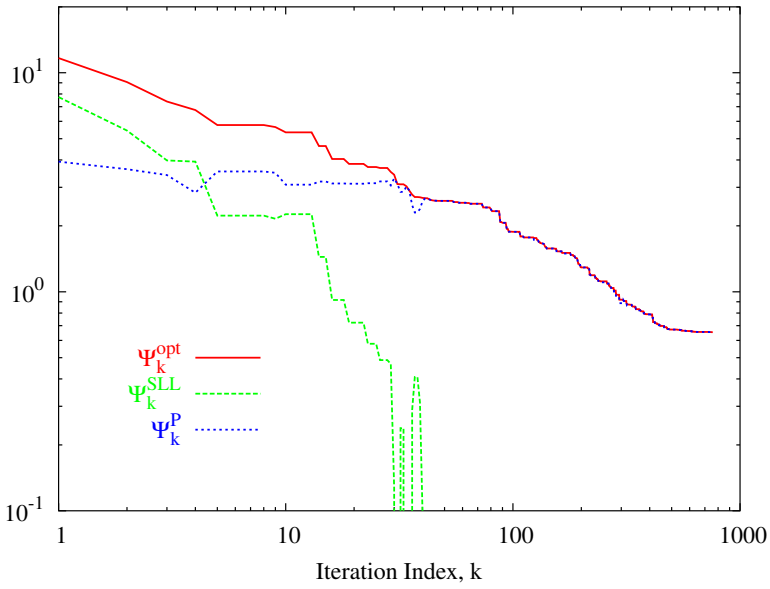

Figure 3.3: *SRs Minimization* ($N = 30$, $d = 0.7\lambda$) - Behavior of the cost function and its terms during the iterative *PSO*-based minimization.

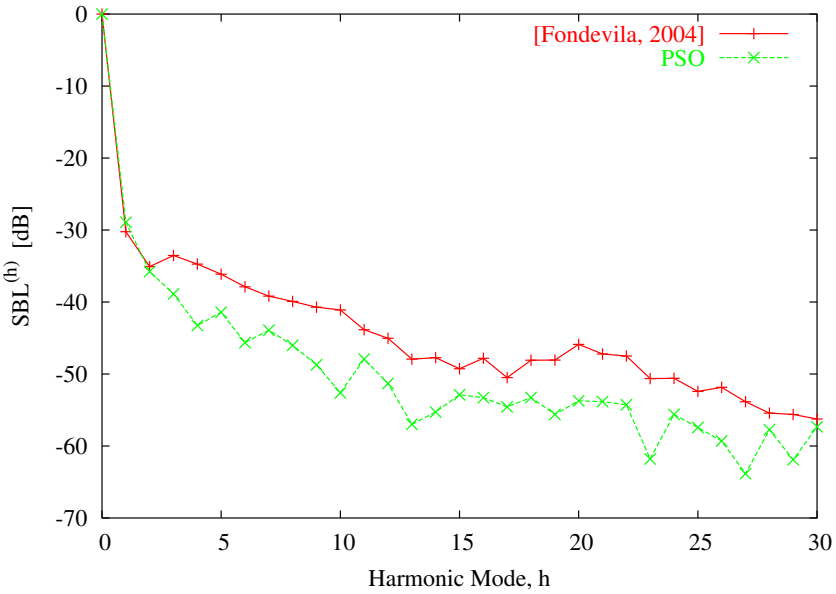

Figure 3.4: *SRs Minimization* ($N = 30$, $d = 0.7\lambda$) - Behavior of the sideband levels $SBL^{(h)}$ when $h \in [0, 30]$. Reference [12] and values computed with the *PSO*-optimized pulse sequence in Figure 3.1.

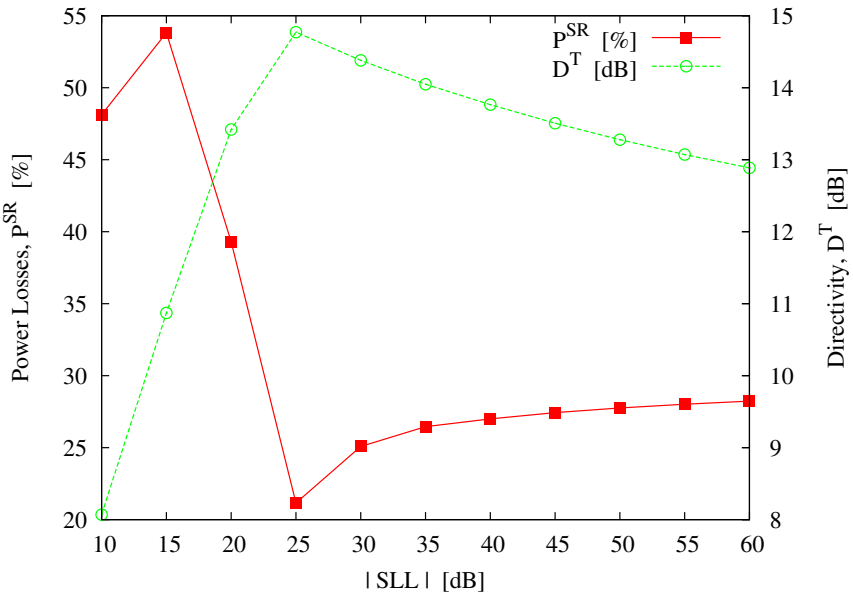

Figure 3.5: *Performance Analysis* ($N = 30$, $d = 0.7\lambda$) - Behavior of the power losses $\mathcal{P}^{SR}$ and directivity D^T versus the SLL for Dolph-Chebyshev patterns [26].

when considering Dolph-Chebyshev distributions [26]. As expected, it is worth noting that there is an inverse relationship between the amount of power losses and the maximum directivity for time-modulated linear arrays.

3.4 Discussions

In this chapter an innovative approach for the synthesis of time-modulated arrays has been proposed. In order to reduce the power losses, a PSO-based strategy has been adopted to minimize a closed-form relationship, that takes into account the whole sideband radiations in direct way and consequently it allows to avoid the computationally-expensive evaluation of the infinite set of harmonic patterns. Thanks to these key-features, the proposed technique represents an improvement with respect to other state-of-art techniques in terms of simplicity and efficiency into reduce the sideband radiations.

Chapter 4

Synthesis of Time-Modulated Planar Arrays

This chapter deals with the minimization of the power losses due to undesired sideband radiations in time-modulated planar arrays. A closed-form expression for computing the total power wasted in the sideband radiations is derived and properly exploited to design a new procedure based on a Particle Swarm Optimizer for the synthesis of the pulse sequences that control the time-modulated array. A set of representative results is shown and analyzed in order to assess the effectiveness of the proposed strategy.

4.1 Introduction

The use of a pulse sequence to modulated the antenna array excitations by means of RF switches has been proved to be a suitable synthesis technique in several applications as the sum and difference antennas [30] and phase switched screens [17] up to airborne pulse doppler radars [29]. As a matter of fact, the improved flexibility of the antenna design allows to generate several patterns with different shapes a [30] and sidelobe levels [3] without the need to change the static excitations represents a non-negligable advantage of time-modulation strategy.

However, the main disadvantage of TM arrays is related to the sideband radiations (SRs) due to the undesired harmonics that arise when the array elements are modulated by a sequence of pulses. To avoid such a drawback, different optmization algorithms have been developed in order to reduce the sideband levels ($SBLs$) (i.e., the peak levels of the harmonic radiations). Approaches based on the Differential Evolution (DE) [8], the Simulated Annealing (SA) [12], the Genetic Algorithm (GA) [13] have been profitably applied. Moreover, a different strategy exploiting time sequences with arbitrary *switch-on* instants has been also presented in [25].

Even if the aformentioned approaches are able to deal efficiently with the SRs in linear array, those strategies do not seem to be suitable to be extended to the synthesis of time-modulated planar arrays ($TMPA$). As a matter of fact, the evaluation of patterns radiated by the undesired harmonics is extremely time-consuming and it cannot be limited at the first harmonic (as it usually done in TM linear arrays) since the losses related with higher frequency harmonics are more relevant because the larger number of elements that usually constitute the planar array.

On the other hand, a simple closed-form relationship that describes the total power wasted by the SRs for linear TM arrays has been developed [5]. Such an expression enables an easy and complete computation of the power losses avoiding the evaluation of the (infinite) set of higher harmonic patterns. Consequently, the proposed approach follows such a philosophy firstly extending the mathematical formulation in [5] to planar arrays and successively developing an explicit form expression that evaluates the power losses.

Accordingly, the outline of the chapter is as follows. In Sect. 4.2 the radiation of time-modulated planar arrays ($TMPA$) is mathematically described and a closed-form relationship for the SRs is determined and minimized by means of a PSO. Successively, in Sect.4.3 a selected results from an exhaustive set of numerical simulations is reported and discussed. Finally, some conclusions are drawn in Sect. 4.4.

4.2 Mathematical Formulation

Let us consider a planar array with $M \times N$ elements displaced on a regular grid along the $x-y$ plane. The *static* set of element excitations $\underline{A} = \{\alpha_{mn};\, m = 0, ..., M-1,\, n = 0, ..., N-1\}$ is modulated by means of periodic rectangular pulse functions generated by RF switches inserted into the antenna feed network to obtain *dynamic* excitations. The array factor is then given by:

$$AF(\theta, \phi, t) = e^{j\omega_0 t} \sum_{m=0}^{M-1} \sum_{n=0}^{N-1} \alpha_{mn} g_{mn}(t)\, e^{j\beta \sin\theta (x_m \cos\phi + y_n \sin\phi)} \tag{4.1}$$

where $x_m = m \times d_x$ and $y_n = n \times d_y$ denote the location of the mn-th array element, $\beta = \frac{\omega_0}{c}$ is the free-space wave number, ω_0 and c being the carrier angular frequency and the speed of light in vacuum, respectively. Moreover, the time behavior of the RF switches is mathematically modeled through the function $g_{mn}(t) = g_{mn}(t + iT_p)$, i and T_p being an integer value and the modulation period, respectively. Then $g_{mn}(t)$ is considered to be:

$$g_{mn}(t) = \begin{cases} 1 & if \;\; 0 < |t| \leq \frac{\widetilde{t}_{mn}}{2} \\ 0 & otherwise \end{cases} . \tag{4.2}$$

As for the linear case, such a periodic function can be expressed in terms of its Fourier coefficients

$$g_{mn}(t) = \sum_{h=-\infty}^{\infty} G_{mnh} e^{jh\omega_p t},\;\; m = 0, ..., M-1,\; n = 0, ..., N-1 \tag{4.3}$$

where $\omega_p = \frac{2\pi}{T_p}$ and G_{mnh} is a real quantity computed to:

$$G_{mnh} = \frac{1}{T_p} \int_{-T_p/2}^{T_p/2} g_{mn}(t) e^{-jh\omega_p t} dt. \tag{4.4}$$

Substituting (4.3) in (4.1) the array factor results a summation of infinite harmonics [5]:

$$AF(\theta, \phi, t) = \sum_{h=-\infty}^{\infty} AF_h(\theta, \phi, t) \tag{4.5}$$

where the h-th harmonic term is given by:

$$AF_h(\theta, \phi, t) = e^{j\omega_0 t} \sum_{m=0}^{M-1} \sum_{n=0}^{N-1} \alpha_{mn} G_{mnh} e^{jk \sin\theta (x_m \cos\phi + y_n \sin\phi)} e^{jh\omega_p t}. \tag{4.6}$$

Then, the pattern at working frequency ($h = 0$) is given by:

$$AF_0(\theta, \phi) = e^{j\omega_0 t} \sum_{m=0}^{M-1} \sum_{n=0}^{N-1} \alpha_{mn} \tau_{mn} e^{j\beta \sin\theta (x_m \cos\phi + y_n \sin\phi)} \tag{4.7}$$

being $\tau_{mn} = \frac{\widetilde{t}_{mn}}{T_p} = G_{mn0}$. Moreover, let us rewrite (4.5) as:

$$AF\left(\theta,\phi,t\right) = \sum_{h=-\infty}^{\infty} \left|\mu_h\left(\theta,\phi\right)\right| e^{j(\omega_0+h\omega_p)t} \tag{4.8}$$

where the term μ_h is computed as:

$$\mu_h\left(\theta,\phi\right) = \sum_{m=0}^{M-1}\sum_{n=0}^{N-1} \alpha_{mn} G_{mnh} e^{j\beta(x_m\cos\phi + y_n\sin\phi)}. \tag{4.9}$$

Now, let us compute the total power radiated by a $TMPA$ as:

$$\mathcal{P}_{TOT} = \frac{1}{T_p}\int_{-T_p/2}^{T_p/2}\left[\int_0^{2\pi}\int_0^{\pi} Re\left\{AF(\theta,\phi,t)\right\}^2 \sin\theta d\theta d\phi\right] dt \tag{4.10}$$

since the following expression holds true [5]:

$$\frac{1}{T_p}\int_{-T_p/2}^{T_p/2} \mathrm{Re}\left\{AF(\theta,\phi,t)\right\}^2 dt = \sum_{h=-\infty}^{\infty} \left|\mu_h(\theta,\phi)\right|^2 \tag{4.11}$$

the power losses associated to the sideband radiations are given by:

$$\mathcal{P}_{SR} = \frac{1}{2}\int_0^{2\pi}\int_0^{\pi} \sum_{h=-\infty,h\neq 0}^{\infty} \left|\mu_h(\theta,\phi)\right|^2 \sin\theta d\theta d\phi. \tag{4.12}$$

Since $\left|\mu_h(\theta,\phi)\right|^2 = \mu_h(\theta,\phi)\left[\mu_h(\theta,\phi)\right]^*$ and taking into account the following relationship from [5]:

$$\sum_{h=-\infty,h\neq 0}^{\infty} G_{mnh}G_{rsh} = \Delta\tau_{mn}^{rs} - \tau_{mn}\tau_{rs} \tag{4.13}$$

where $\Delta\tau_{mn}^{rs} = \tau_{mn}$ if $\tau_{mn} \leq \tau_{rs}$ and $\Delta\tau_{mn}^{rs} = \tau_{rs}$ otherwise, Equation (4.12) can be rewritten as follows:

$$\begin{aligned}\mathcal{P}_{SR} \;=\; & 2\pi\sum_{m=0}^{M-1}\sum_{n=0}^{N-1}\sum_{r=0}^{M-1}\sum_{s=0}^{N-1}\Bigg[Re\left\{\alpha_{mn}\alpha_{rs}^*\right\}\cdot \\ & \frac{\sin\left(\beta\sqrt{(x_m-x_r)^2+(y_n-y_s)^2}\right)}{\beta\sqrt{(x_m-x_r)^2+(y_n-y_s)^2}}\left(\Delta\tau_{mn,rs} - \tau_{mn}\tau_{rs}\right)\Bigg]\end{aligned} \tag{4.14}$$

after simple manipulations detailed in **Appendix** A. Moreover, for a square $(N\times N)$ planar arrays, Equation (4.14) simplifies to:

$$\begin{aligned}\mathcal{P}_{SR} &= 2\pi \sum_{m,\,n=0}^{N-1} \left[|\alpha_{mn}|^2 \tau_{mn}(1-\tau_{mn})\right] + \\ & 2\pi \sum_{m,\,n=0,\,(r,s)\neq(m,n)}^{N-1} \left[Re\left\{\alpha_{mn}\alpha_{rs}^*\right\} \cdot \right. \\ & \left. \frac{\sin\left(\beta\sqrt{(x_m-x_r)^2+(y_n-y_s)^2}\right)}{\beta\sqrt{(x_m-x_r)^2+(y_n-y_s)^2}} \left(\Delta\tau_{mn,rs} - \tau_{mn}\tau_{rs}\right)\right]\end{aligned} \tag{4.15}$$

4.2.1 PSO-based Power Losses Minimization

The analytic form of $\mathcal{P}_{SR}$ [Eq. (4.14)-(4.15)] enables a computationally-efficient optimization of the power losses in $TMPA$s. Towards this end, the problem unknowns are the *static* excitation coefficients, $\underline{A} = \{\alpha_{mn};\, m = 0, ..., M-1,\, n = 0, ..., N-1\}$, and the set of *switch-on times*, $\underline{\tau} = \{\tau_{mn};\, m = 0, ..., M-1,\, n = 0, ..., N-1\}$. Let us assume a fixed set of *static* excitations, $\underline{A} = \hat{\underline{A}}$. Therefore, the use of time-pulses would allow an initial pattern (generated by the static excitation distribution) to be reconfigured by the insertion of the on-off switches between the generator and the array elements, avoiding a new feeding network design that would be necessary if time-modulation were not applied. The minimization of the losses is then recast as the solution of an equivalent optimization problem mathematically formulated in terms of the following cost function

$$\begin{aligned}\Psi\left\{\underline{\tau}_k\right\} &= w_{SLL} H\left[\widetilde{SLL} - SLL\left(\underline{\tau}_k\right)\right] \frac{\left|\widetilde{SLL} - SLL(\underline{\tau}_k)\right|^2}{\left|\widetilde{SLL}\right|^2} \\ & + w_{SR} \frac{\mathcal{P}_{SR}(\underline{\tau}_k)}{\mathcal{P}_{TOT}(\underline{\tau}_k)}\end{aligned} \tag{4.16}$$

and aimed at defining the optimal set $\underline{\tau}_{opt}$ at the convergence of an iterative process, k being the iteration index. Moreover, $H(\cdot)$ is the Heaviside step function, while w_{SLL} and w_{SR} are real and positive weights. The first term in (4.16), Ψ_{SLL}, penalizes the mismatch between the sidelobe level generated at $h = 0$ by $\underline{\tau}_k$, $SLL\left(\underline{\tau}_k\right)$, and the desired one, $\widetilde{SLL}$, whether $SLL\left(\underline{\tau}_k\right) > \widetilde{SLL}$. It acts like a constraint of the minimization of the power losses forced by the other term, Ψ_{SR}.

Since the unknown set $\underline{\tau}_k$ is real-valued, the minimization of (4.16) is carried out by means of a Particle Swarm Optimizer (PSO) [18] whose implementation is detailed in [27]. The iterative process stops when a maximum number of iterations K is reached or at the stationariness of the value of $\Psi_k^{opt} = \Psi\left\{\underline{\tau}_k^{opt}\right\}$, $\underline{\tau}_k^{opt} = arg\left\{\min_{s=1,...,S}\left[\Psi\left(\underline{\tau}_k^{(s)}\right)\right]\right\}$, S being the number of particles/agents of the swarm.

4.3 Numerical Validation

A set of representative results is here reported to show the potentialities of the proposed method for the synthesis of $TMPA$ with reduced SRs. The first example deals with a planar array having circular contour, while the second one is concerned with the synthesis of a rectangular arrangement. As regards the PSO, the control parameters have been set to the values derived in [27], namely $\omega = 0.4$ (inertial weight), $C_1 = 2.0$ (cognitive acceleration coefficient), $C_2 = 2.0$ (social acceleration coefficient).

In the first example, the array elements are placed on a regular grid of dimension $N \times M = 20 \times 20$ with inter-elements spacing equal to $d_x = d_y = 0.5\lambda$ and the antenna contour has radius $r = 5\lambda$, $\lambda = cT_0$ being the free space wavelength. Thus, the number of radiating array elements amounts to $L = 316$, while the other 84 elements laying outside the circular contour are deleted from the grid (i.e., $\alpha_{mn} = 0$). Starting from a set of *static* excitation $\underline{\hat{A}}$ obtained through the sampling of the Taylor distribution ($SLL = -30\,dB$, $\bar{n} = 6$ [31]) and affording a pattern with $SLL = -29.25\,dB$ [32] and because of the quadrantal symmetry of the array architecture, a quarter of the total number of elements, $U = 79$, has been optimized for the synthesis of a broadside pencil beam pattern. The cost function (4.16) has been then minimized with a swarm of $S = 30$ particles. The value $\widetilde{SLL}$ has been set to $-40\,dB$ and the weight coefficients have been heuristically tuned to $w_{SLL} = 2$ and $w_{SR} = 1$. Moreover, $K = 2000$ iterations have been considered and, at the initialization, the *switch-on times* have been randomly-generated with uniform probability within $\tau_{mn}^{(0)} \in [0, 1]$, $\forall(m, n)$.
The normalized power pattern generated at the central frequency is shown in Figure 4.1. The level of the secondary lobes is reduced of almost $8\,dB$ ($SLL_{opt} = -37.8\,dB$) compared to that afforded with the *static* excitations and the power wasted in SRs amounts to $\mathcal{P}_{SR} = 13.2\%$ of the total input power. The PSO-optimized pulse sequence $\underline{\tau}_{opt}$ is reported in Figure 4.2 (a) together with the distribution of the static excitations [Figure 4.2 (b)].
For completeness, the behavior of the cost function Ψ_k^{opt} along the iterative optimization process is shown in Figure 4.3 while the patterns at the first ($|h| = 1$) and the second ($|h| = 2$) harmonics are shown in Figure 4.4(a) and Figure 4.4 (b), respectively.

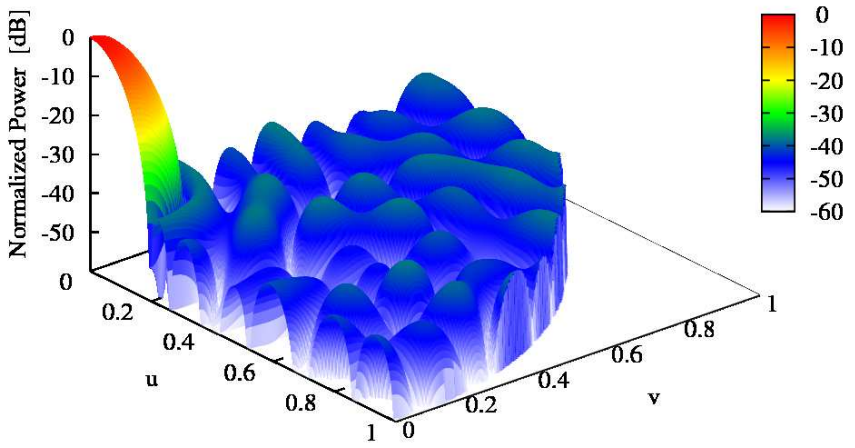

Figure 4.1: *Circular Aperture* ($N = M = 20$, $L = 316$, Taylor [31] $SLL = -30\,dB$, $\bar{n} = 6$) - Normalized power pattern at the carrier frequency ($h = 0$).

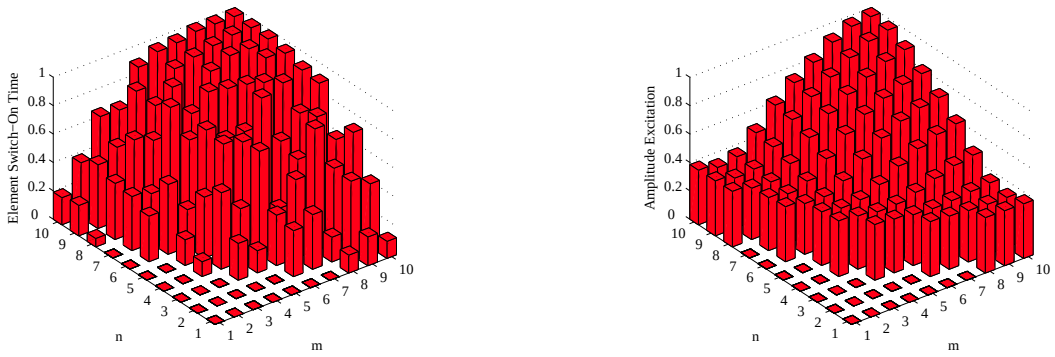

(a) (b)

Figure 4.2: *Circular Aperture* ($N = M = 20$, $L = 316$, Taylor [31] $SLL = -30\,dB$, $\bar{n} = 6$) - Distribution of (a) the optimized switch-on times and (b) the static element excitations.

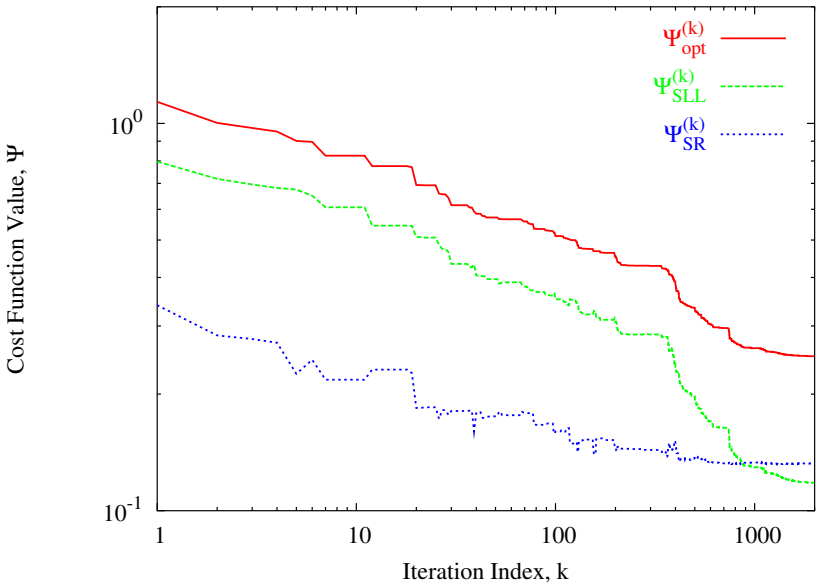

Figure 4.3: *Circular Aperture* ($N = M = 20$, $L = 316$, Taylor [31] $SLL = -30\,dB$, $\bar{n} = 6$) - Behavior of the cost function terms during the iterative *PSO*-based optimization.

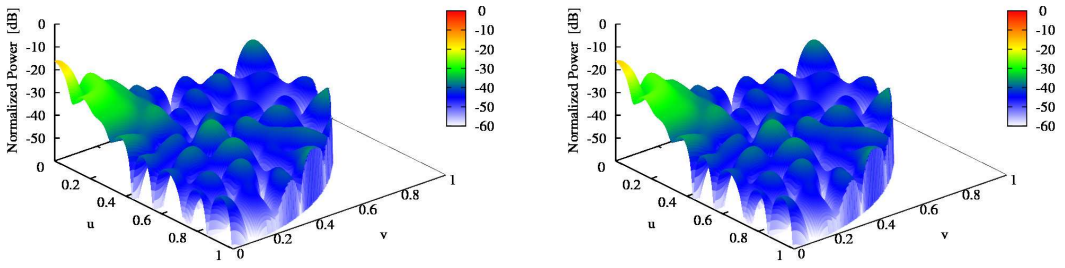

(a) (b)

Figure 4.4: *Circular Aperture* ($N = M = 20$, $L = 316$, Taylor [31] $SLL = -30\,dB$, $\bar{n} = 6$) - Normalized power patterns at (a) the first ($h = 1$) and (b) the second ($h = 2$) harmonics.

The second test deals with a square array with $N \times M = 10 \times 10$ elements located on the same grid of the previous example. In this case, the *static* element excitations are uniformly-distributed: $\alpha_{mn} = 1, \forall\,(m,n)$. The array factor at $h = 0$ can be expressed either through (4.7) or, assuming the *separable distribution* condition for the dynamic excitations, as the product of the array factors of two linear arrays of M and N elements along the x and y axes, respectively

$$AF_0(\theta,\phi) = \sum_{m=0}^{M-1} \alpha_m \tau_m e^{j\beta x_m sin\theta cos\phi} \sum_{n=0}^{N-1} \alpha_n \tau_n e^{j\beta y_n sin\theta sin\phi}. \tag{4.17}$$

Moreover, the following relationships hold true

$$\alpha_m \tau_m = \frac{\alpha_{m0}\tau_{m0}}{\alpha_{00}\tau_{00}}\ ,\ \alpha_n \tau_n = \frac{\alpha_{0n}\tau_{0n}}{\alpha_{00}\tau_{00}} \tag{4.18}$$

$m = 0, ..., M-1$ and $n = 0, ..., N-1$.

The number of unknowns in the non-separable case [Eq. (4.14)] is equal to $U = 25$ (i.e., a quarter of the total number of elements $L = 100$), while the separable case [Eq. (4.15)] considers only $U = 10$ variables. As regards the optimization, a swarm of $S = 15$ particles has been used with a maximum number of iterations equal to $K = 1000$. Moreover, the constraint on the sideband level has been set to $\widetilde{SLL} = -20\,dB$.

At the end of the PSO-based optimization, the patterns in Figure 4.5 (a) and Figure 4.5 (b) have been synthesized for the non-separable case (NSD) and the separable one (SD), respectively. The level of the sidelobes is equal to $SLL_{NSD} = -19.6\,dB$ and $SLL_{SD} = -19.4\,dB$, respectively. Moreover, the secondary lobes behave differently (Figure 4.5). As expected, higher levels verify along the orthogonal axis of the array (i.e., the x and y axes) in correspondence with the separable distribution [Figure 4.5 (b)]. On the contrary, the energy wasted outside the main lobe is more uniformly-distributed within the visible range in Figure 4.5 (a).

The optimized time-sequences are shown in Figure 4.6. More in detail, Figure 4.6 (a) shows that 6 among 25 elements are switched-off, while the *switch-on times* of the separable distribution [Figure 4.6(b)] satisfy (4.15).

Thanks to the larger number of degrees of freedom ($U_{NSD} = 25$ vs. $U_{SD} = 6$), the power losses in the SRs result lower than 3% (i.e., $\mathcal{P}_{SR} = 2.8\%$), while they rise to $\mathcal{P}_{SR} = 11.1\%$ for the pattern synthesized with the optimized separable distribution. The non-negligible reduction of $\mathcal{P}_{SR}$ has also a positive effect on the SBLs of the harmonic radiations. Figure 4.7 shows the patterns generated by the pulse sequence in Figures 4.6(a)-4.6(b) at the first ($|h| = 1$) [Figures 4.7(a)-(b)] and the second ($|h| = 2$) [Figures 4.7(c)-(d)] harmonic terms. The SBLs of the patterns generated optimizing $U_{NSD} = 25$ elements [Figures 4.7(a)-(c)] are much lower than those obtained when $U_{SD} = 10$ [Figures 4.7(b)-(d)]. More specifically, $SBL^{(1)}_{NSD} = -31.8\,dB$ vs. $SLL^{(2)}_{SD} = -20.2\,dB$ and $SBL^{(1)}_{NSD} = -33.1\,dB$ vs. $SLL^{(2)}_{SD} = -22.9\,dB$. For completeness, the values of the SBLs until $h = 20$ are reported in Figure 4.8.

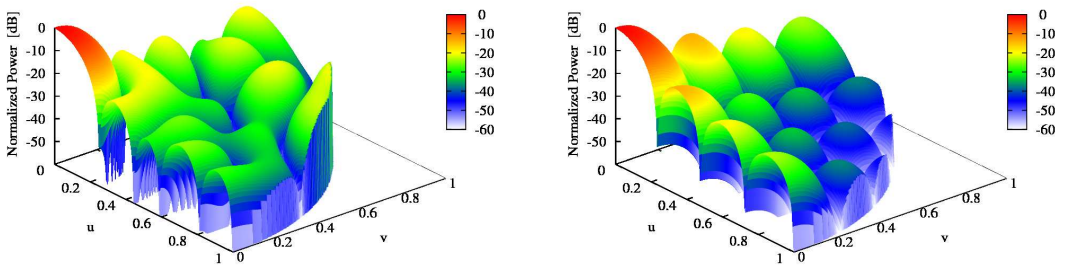

(a) (b)

Figure 4.5: *Rectangular Aperture* ($N = M = 10$, $L = 100$, $\alpha_{mn} = 1$) - Normalized power patterns at the carrier frequency ($h = 0$) for (a) the non-separable case and (b) the separable one.

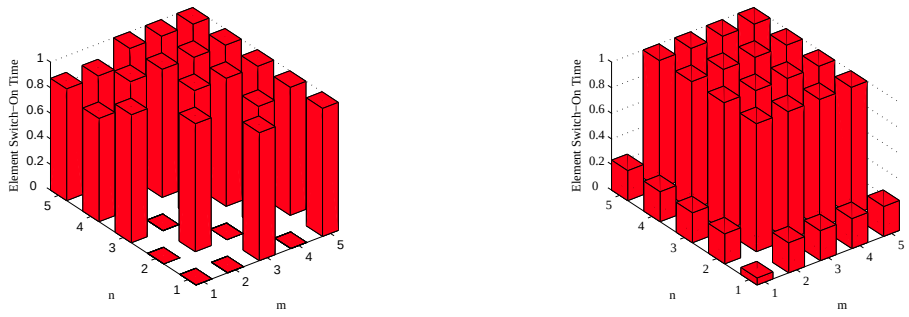

(a) (b)

Figure 4.6: *Rectangular Aperture* ($N = M = 10$, $L = 100$, $\alpha_{mn} = 1$) - Distribution of the optimized switch-on times for (a) the non-separable and (b) the separable cases.

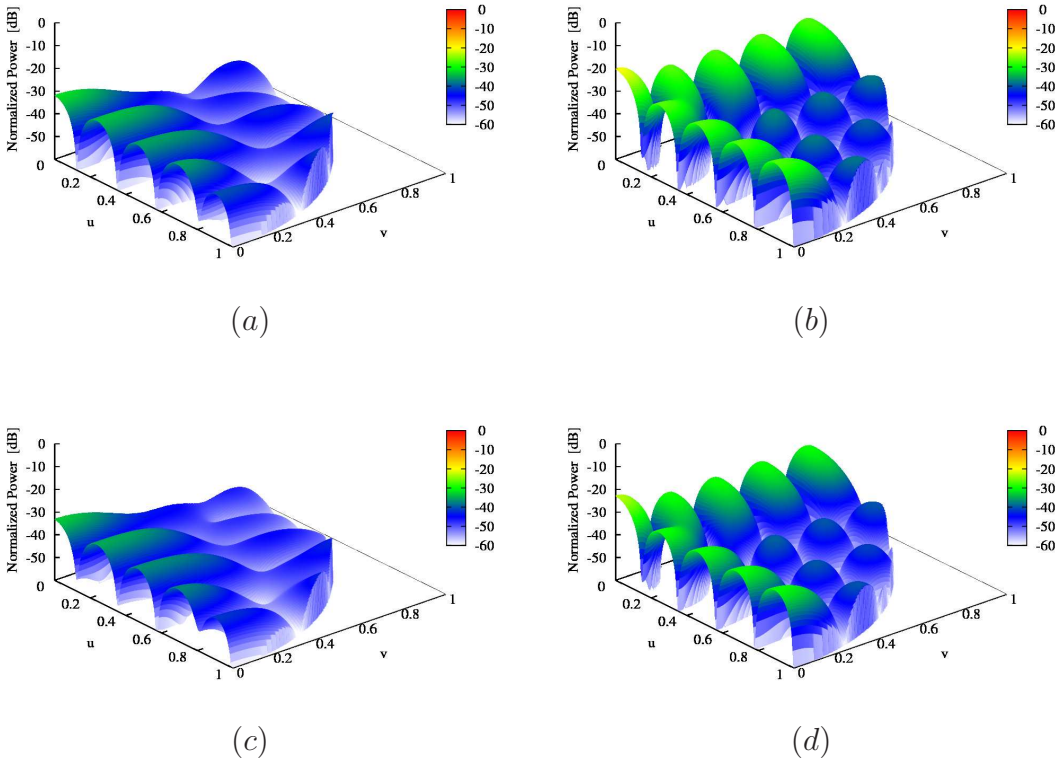

Figure 4.7: *Rectangular Aperture* ($N = M = 10$, $L = 100$, $\alpha_{mn} = 1$) - Normalized power patterns at $(a)(b)$ the first ($|h| = 1$) and $(c)(d)$ the second ($|h| = 2$) terms in correspondence with $(a)(c)$ the NSD case and $(b)(d)$ the SD one.

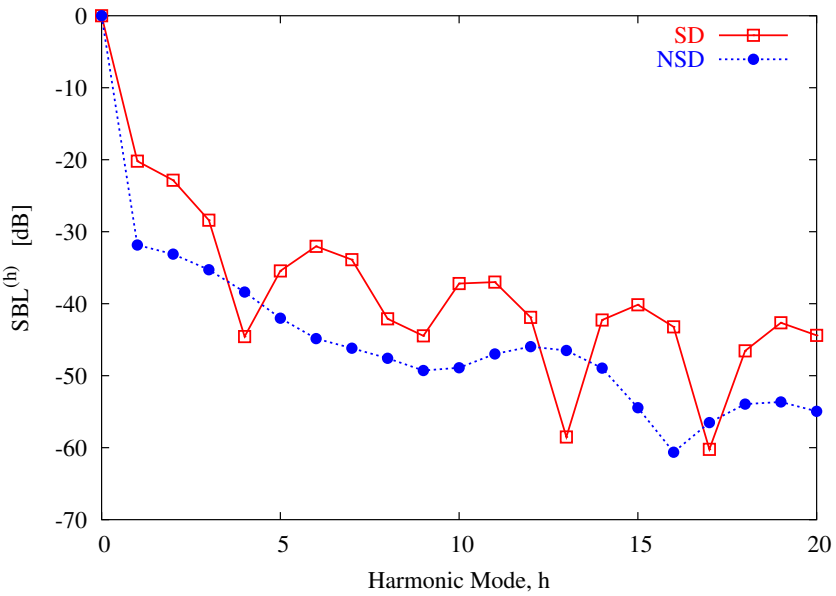

Figure 4.8: *Rectangular Aperture* ($N = M = 10$, $L = 100$, $\alpha_{mn} = 1$) - Behavior of the sideband levels, $SBL^{(h)}$, $h \in [0, 20]$, of the solutions synthesized in the NSD and the SD cases.

As far as the iterative minimization is concerned, the convergence has been yielded in the separable case only after 226 iterations, while the maximum number of iterations ($K = 1000$) have been necessary otherwise to get the final solution because of the wider solution space to be sampled during the optimization.

4.4 Discussions

In this chapter, the reduction of the power losses due to SRs has been carried out by means of an effective PSO-based strategy thanks to the definition of a closed-form relationship that allows a complete computation of the power losses of the undesired harmonics. The obtained results have shown the effectiveness of the proposed method as a realible alternative to other state-of-art techniques aimed at optimizing the $SBLs$ at first harmonic term. The approach has been analyzed both for separable and non-separable coefficient distributions in order to point out that the sideband radiations can be effectively reduced exploiting a larger number of degree of freedom, but at the cost of an increased computational burden.

Chapter 5

Synthesis of Compromise Sum-Difference Arrays through Time-Modulation

In this chapter the time-modulation is exploited for the synthesis of monopulse subarrayed antennas. The solution of the sum-difference compromise problem is achieved by setting the set of static excitations to an optimal sum set and synthetizing the "best compromise" difference pattern through a Contiguous Partition Method (CPM) based approach. The array elements are aggregated into sub-arrays controlled by means of RF switches with optimized "on" time-durations. The switch-on instants of the pulse sequence are then computed by means of a Particle Swarm Optimizer to reduce the waste of power caused by the sideband radiations. A selected set of numerical results is reported in order to assess the potentialities of the time-modulation to deal with the problem in hand.

5.1 Introduction

Search-and-track radars based on monopulse principles require antenna systems generating sum and difference patterns. In the scientific literature, several approaches refer to the frequency domain and consider fixed antenna geometries as well as the exploitation of the degrees of freedom available in both the frequency domain and the spatial domain. Analytical procedures aimed at computing in an "optimal" way the excitation weights of the array elements belong to the former class. Patterns with either equi-ripple [26][33] or tapered [34][35] sidelobes have been efficiently obtained. Other strategies for the optimal synthesis of power patterns with arbitrary sidelobe bounds have been proposed [36][37][38], as well. In those approaches optimal patterns in the Dolph-Chebyshev sense have been determined. They realize an optimal trade-off between the sidelobe level (SLL) and the main lobe beamwidth (BW) or between the BW and the deepness of the slope along the boresight direction for a fixed SLL when dealing with sum patterns or difference patterns, respectively. Although the synthesis of optimal beams allows one to increase the resolution capability (i.e., a narrow BW and a deep boresight slope) and to enhance the reliability of the search and track system (i.e, a low SLL), it also requires the use of two independent feed networks.

In order to limit such a complexity constraint, additional degrees of freedom have been introduced by considering a partial sharing of the antenna circuitry between the two beams. In this framework, sub-arraying has been used [39] to approximate, in the least square sense, both sum and difference patterns starting from reference excitations. Towards this end, Taylor [40] and Bayliss [41] continuous distributions have been considered in [42] to optimize difference patterns by means of a Simulated Annealing (SA) algorithm. Moreover, following the guidelines originally presented by McNamara in [20], a growing attention has been also devoted to synthesize optimal compromise sum and difference patterns using sub-arrayed arrays. In such a case, the optimal sum pattern is usually generated through an independent beam-forming network, whereas the sub-optimal difference one is obtained spatially aggregating the elements into sub-arrays and assigning a suitable weight to each of them. Towards this purpose, analytical procedures [20][21], stochastic optimization algorithms [43][44][45][46], and hybrid methods [47][48] have been successfully applied.

Dealing with compromise solutions, this paper presents a new strategy aimed at exploiting time as an additional degree of freedom for the synthesis of difference patterns in sub-arrayed array antennas. Thanks to the use of RF switches, the approach enforces time-modulation to the static element excitations. Originally, time-modulation has been used for the synthesis of low and ultra-low sidelobe arrays for radar applications [3] and communication purposes [4]. More recently, some studies have been carried out to extend the application of time-modulation to other antenna synthesis problems. For instance, difference patterns have been synthesized by time-modulating a small number of elements of a two-section array

generating a sum pattern [30]. However, even though pioneering works concerned with time-modulation date back to the end of 1950s [1], the potentialities of time-modulated arrays have been only partially investigated. This has been mainly due to the presence of undesired sideband radiations (SRs) which unavoidably affect the performance of time-modulated arrays. In order to minimize the SR power losses, different approaches based on evolutionary optimization algorithms have been proposed [8][9][12][13]. Otherwise, it has been demonstrated in [25] that the control of the sideband levels at the harmonic frequencies can be yielded by using suitable switching strategies providing effective pulse sequences.
In this paper, a time-modulation strategy is proposed as a suitable alternative to standard compromise methods, which neglect the time variable in the design process, to synthesize compromise arrays. Starting from a set of static excitations generating an optimal sum pattern at the carrier frequency, a compromise difference beam is synthesized through a sub-arraying pattern matching procedure [21] aimed at optimizing the pulse durations at the input ports of the sub-arrays. Successively, the SRs at the harmonic frequencies are minimized by performing a Particle Swarm Optimization (PSO) to set the switch-on instants of the time sequences.
Accordingly, the outline of the chapter is the following. The compromise problem is mathematically described in Sect. 5.2 where the pattern matching procedure as well as the strategy for the sideband level (SBL) minimization are also outlined. A selected set of numerical experiments are reported and discussed in Sect. 5.3 to point out advantages and limitations of the proposed technique. Finally, some conclusions are pointed out (Sect. 5.4).

5.2 Mathematical Formulation

Let us consider a two-section linear array [49] of $N = 2 \times M$ elements equally-spaced (d being the inter-element distance) along the x-axis. According to the guidelines of the sub-arraying technique [20], the static real excitation coefficients $\mathbf{A} = \{\alpha_m = \alpha_{-m};\ m = 1, ..., M\}$ affording the sum pattern AF_Σ:

$$AF_\Sigma(\theta;\ \mathbf{A}) = 2\sum_{m=1}^{M} \alpha_m \cos\left[\left(m - \frac{1}{2}\right) kd\sin\theta\right] \tag{5.1}$$

are computed using optimal techniques (e.g., [26][34][36]). Moreover, θ is the angular direction with respect to the array axis and $k = \frac{\omega_0}{c}$ is the wavenumber, ω_0 and c being the angular carrier frequency and the speed of light, respectively. To generate the compromise difference patterns, the array elements are grouped into $R = 2 \times Q$ sub-arrays (i.e., Q for each half of the array). At each sub-array port, an RF switch is used to modulate the excitations of the elements assigned to the sub-array (Fig. 5.1). Mathematically, the process of enforcing a time-modulation to the sub-array signals can be described by defining a set of Q rectangular functions

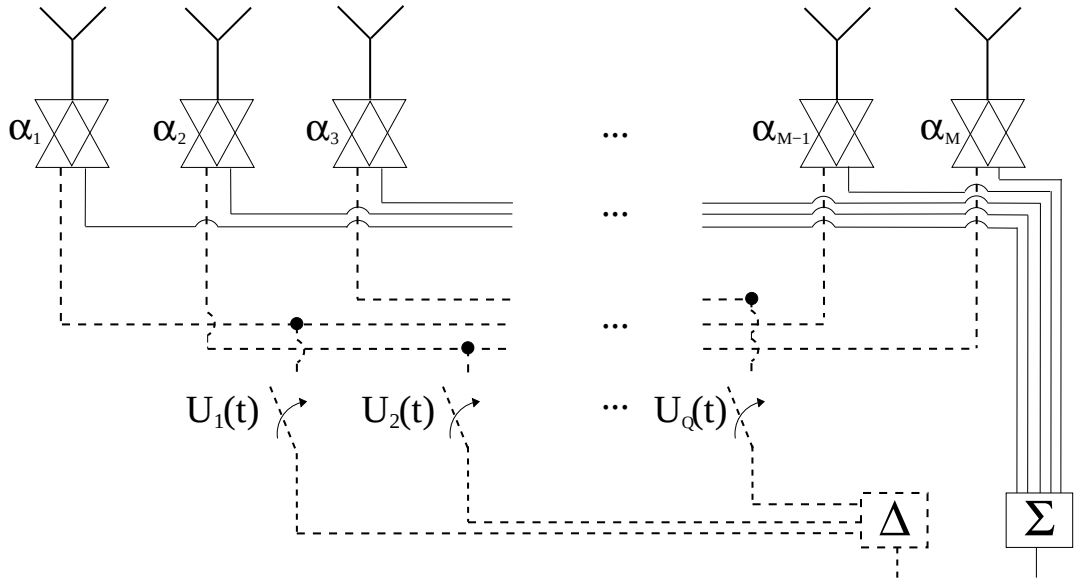

Figure 5.1: *Monopulse sub-arrayed* antenna - Sketch of the antenna feed network.

$$U_q(t) = \begin{cases} 1 & t_q^{on} \le t \le t_q^{off} \\ 0 & otherwise \end{cases}, \quad q = 1, ..., Q \tag{5.2}$$

t_q^{on} and t_q^{off} being the sub-array *switch-on instant* and the *switch-off instant* of the q-th sub-array, respectively. The values of t_q^{on} and t_q^{off}, $q = 1, ..., Q$, are additional degrees of freedom to be determined for approximating the desired/reference difference pattern.
Since these rectangular pulses are periodic in time (with period T_p), each function $U_q(t)$, $q = 1, ..., Q$, is then expanded into its Fourier series and the condition $T_p \gg T_o = \frac{2\pi}{\omega_0}$ is assumed to hold true. It is then simple to show [3] that the arising expression of the array factor is composed by an infinite number of frequency components centered at ω_0 and separated by $h\omega_p = h\frac{2\pi}{T_p}$, h being the harmonic index. Let us choose to synthesize the difference pattern at the carrier frequency ($h = 0$). Accordingly, it results that

$$AF_{\Delta}^{(0)}(\theta;\, \mathbf{C},\, \mathbf{T}) = 2\sum_{m=1}^{M} \alpha_m \sum_{q=1}^{Q} \tau_q \delta_{c_m q} \sin\left[\left(m - \frac{1}{2}\right) kd \sin\theta\right] \tag{5.3}$$

where $\mathbf{T} = \{\tau_q;\, q = 1, ..., Q\}$ is the set of 0-th order Fourier coefficients (also called *normalized switch-on times*) given by

$$\begin{aligned} \tau_q &= u_{hq}\big\rfloor_{h=0} \triangleq \frac{1}{T_p}\int_0^{T_p} U_n(t)\, e^{-jh\omega_p t} dt\Big|_{h=0} \\ &= \frac{t_q^{off} - t_q^{on}}{T_p}, \quad q = 1, ..., Q, \end{aligned} \tag{5.4}$$

where $\delta_{c_m q}$ stands for the Kronecker delta function and $\mathbf{C} = \{c_m \in [0,\, Q]\,;\, m = 1,$

$..., M\}$ is the integer vector describing the sub-array configuration. As an example, $c_m = 0$ means that the excitation of the m-th element is not time-modulated. In order to synthesize a compromise difference pattern close to a reference/optimal one, the definition of the two sets of unknowns $\mathbf{C}$ and $\mathbf{T}$ in (5.3) is then required. Towards this end, a suitable state-of-the-art sub-arraying procedure is used following the guidelines of the pattern matching procedure presented in [21]. More in detail, the following cost function

$$\Psi^{(0)}\left(\mathbf{C},\,\mathbf{T}\right) = \frac{1}{M}\sum_{m=1}^{M}\left\|\alpha_m\left(\frac{\beta_m}{\alpha_m} - \sum_{q=1}^{Q}\delta_{c_m q}\tau_q\right)\right\|^2 \tag{5.5}$$

is minimized by means of the *Contiguous Partition Method* (CPM) [21], where $\mathbf{B} = \{\beta_m = -\beta_{-m} \;\; m = 1, ..., M\}$ is the set of reference/optimal excitation coefficients [33][35][37] that generate the reference difference pattern to match. As a matter of fact, a suitable customization of the CPM can be effectively used here starting from the key observation that the optimal and independent (when N RF switches are available) values of the switch-on times affording the desired pattern at ω_0 can be exactly computed by means of the techniques in [26][33][34][35][36][37][38]. Hence, the optimal excitation matching problem dealt with in [21] can be reformulated here as an optimal pulse matching problem. Accordingly, once the number of sub-arrays Q is given, the minimization of (5.5) allows to determine the number of elements within each group and the sub-array architecture where the cost function (5.5) is representative of a least square problem measuring the mismatch between the *optimal weights* $\frac{\beta_m}{\alpha_m}$, $m = 1, ..., M$, and the corresponding (unknown) *sub-array switch-on times* τ_q, $q = 1, ..., Q$. For the sake of clarity in the notation, let us indicate with τ_q^{CPM}, $q = 1, ..., Q$, and c_m^{CPM}, $m = 1, ..., M$, the values of the unknowns computed by minimizing (5.5) through the CPM.

It is worth noting that whether, on one hand, the "best compromise" difference pattern at ω_0 can be easily obtained by applying the CPM procedure, on the other hand, SRs are still present because of the commutation between the on and off state of RF switches that controls the time-modulation process. In order to reduce the interferences due to SRs, the optimization of $\mathbf{T}$ in uniform arrays [12] or the joint optimization of both $\mathbf{T}$ and $\mathbf{A}$ [8] has been performed in the literature. However, it should be pointed out [Eq. (5.3)] that a modification of the pulse durations τ_q^{CPM}, $q = 1, ..., Q$, causes the radiation of a different compromise difference pattern and no more the "best compromise" solution obtained through the CPM. Moreover, the static excitation vector $\mathbf{A}$ is *a-priori* fixed to generate the optimal sum pattern. Thus, neither $\mathbf{T}$ nor $\mathbf{A}$ can be now changed to address the SR minimization problem.

Towards this purpose, let us observe that the h-th Fourier coefficient ($h \neq 0$) is equal to

$$u_{hq} \triangleq \frac{1}{T_p}\int_0^{T_p} U_n\left(t\right) e^{-jh\omega_p t} dt = \frac{e^{-jh\omega_p t_q^{off}} - e^{-jh\omega_p t_q^{on}}}{2jh\pi} \tag{5.6}$$

and the corresponding harmonic pattern turns out to be:

$$AF_{\Delta}^{(h)}\left(\theta;\,\mathbf{C},\,\mathbf{U}_h\right) = 2\,e^{j(h\omega_p+\omega_0)t}\sum_{m=1}^{M}\alpha_m\cdot \cdot\sum_{q=1}^{Q}u_{hq}\delta_{c_m q}\sin\left[\left(m-\tfrac{1}{2}\right)kd\sin\theta\right],\;\; |h|=1,...,\infty \tag{5.7}$$

where $\mathbf{U}_h=\{u_{hq};\,q=1,...,Q\}=\mathcal{F}\left(\mathbf{T}^{CPM},\,\mathbf{T}^{on}\right)$ depends on the switch-on time $\mathbf{T}^{CPM}=\left\{\tau_q^{CPM};\,q=1,...,Q\right\}$ and the switch-on instants $\mathbf{T}^{on}=\left\{t_q^{on};\,q=1,...,Q\right\}$, since $t_q^{off}=\tau_q^{CPM}T_p+t_q^{on}$ [Eq. (5.4)]. Therefore, the set $\mathbf{T}^{on}$ can be profitably optimized to reduce the sideband level (SBL) of the harmonic radiations without modifying the pattern at the carrier frequency (i.e., $\mathbf{A}$ and $\mathbf{T}^{CPM}$). A strategy based on a Particle Swarm Optimizer (PSO) [18][23] is then applied to minimize the following cost function

$$\Psi\left(\mathbf{T}^{on}\right)|_{\mathbf{T}=\mathbf{T}^{CPM}} = \sum_{h=1}^{H}\left\{\aleph\left[SBL^{ref}-SBL^{(h)}\left(\mathbf{T}^{on}\right)\right]\left|\Delta_{SBL}^{(h)}\left(\mathbf{T}^{on}\right)\right|^2\right\} \tag{5.8}$$

where $\Delta_{SBL}^{(h)}\left(\mathbf{T}^{on}\right)=\frac{SBL^{ref}-SBL^{(h)}(\mathbf{T}^{on})}{SBL^{ref}}$ and $\aleph(\cdot)$ is the Heaviside function devoted to quantify the distance between the actual harmonic sideband levels, $SBL^{(h)}=SBL\left(\omega_0+h\omega_p\right)$[1], $h=1,...,H$ and the user-defined threshold SBL^{ref}.

5.3 Numerical Validation

In order to discuss the potentialities and current limitations of the proposed approach, the results from two representative experiments are analyzed. More specifically, the same array geometry is considered in both cases, but different static (sum) excitations as well as different numbers of sub-arrays have been used. Since this is the first (to the best of the authors' knowledge) application of the time-modulation to the synthesis of monopulse sub-arrayed antenna where the sum and the difference patterns are simultaneously generated, no comparisons with other methods are possible. However, since the independent generation of difference patterns by modulating a limited number of static excitations that afford a Villeneuve sum pattern has been described in [30], similar scenarios have been considered as reference geometries. Accordingly, let us refer to a $N=30$ element array with inter-element spacing $d=0.7\lambda$ [30]. In the first experiment (*Experiment 1*), the set of static sum excitations $\mathbf{A}$ has been chosen to synthesize a Villeneuve sum pattern with $SLL=-20\,dB$, $\overline{n}=3$ and $\nu=0$ [35]. To generate the compromise difference pattern, $R=8$ sub-arrays have been used

[1] $SBL^{(h)}\triangleq max_\theta\left\{AF_{\Delta}^{(h)}\left(\theta\right)\right\}$

	$\mathbf{C} = \{c_m;\ m = 1, ..., M\}$
$M = 15,\ Q = 4$	1 1 2 3 4 0 0 0 0 0 4 3 2 2 1
$M = 15,\ Q = 2$	1 1 2 2 2 0 0 0 0 0 0 0 0 0 0

Table 5.1: Sub-array configurations for the compromise difference patterns when $Q = 4$ and $Q = 2$.

as in [30] (Tab. 4 - Case B). The CPM has been run by setting the reference difference excitations to those of a Modified Zolotarev pattern [35] with $SLL = -30\,dB$ and $\overline{n} = 5$. The "best compromise" solution, obtained after 16 iterations in $1.7 \times 10^{-5}\,[sec]$ (on a $3\,GHz$ PC with $1\,GB$ of RAM), is shown in Fig. 5.2(a) together with the reference difference pattern. The corresponding element switch-on times, $\mathbf{T}^{CPM}$, and the sub-array configuration $\mathbf{C}^{CPM}$ computed through the minimization of (5.8) are shown in Figure 5.2 (b) and reported in Table 5.1, respectively. For completeness, the plot of the reference excitations is displayed in Figure 5.2 (b) (dotted line). From Figure 5.2 (b), it can be seen that there is a good matching between the main lobes of the reference and compromise difference patterns. As a matter of fact, the $-3\,dB$ beamwidth (BW) is equal to $BW^{ref} = 2.57^o\,[deg]$ and $BW^{CPM} = 2.58^o\,[deg]$, respectively. Therefore, the resolution capability of the monopulse tracking systems (i.e., the deepness of the main lobe along the boresight direction [50]) is kept almost unaltered. Secondly, although the envelope of the secondary lobes is no more decaying as $\frac{1}{sin\theta}$ as for the reference pattern, the SLL of the compromise pattern is close to the optimal one ($SLL^{CPM} = -26.9\,dB$ vs. $SLL^{ref} = -30.0\,dB$) with still a satisfactory ability to suppress interferences and clutters [19].
As far as the CPM solution is concerned, $N_{TM} = 20$ elements over $N = 30$ are time-modulated, while the others are kept time-constant and set to the corresponding static sum excitations (Table 5.1). Concerning SRs, Figure 5.3 shows the patterns radiated at $|h| = 1, 2$. As it can be observed, the highest lobes principally lie in the angular region close to that of the main difference lobes and the values of the $SBLs$ turn out to be $SBL^{(1)}_{CPM} = -14.9\,dB$ and $SBL^{(2)}_{CPM} = -22.4\,dB$, respectively. In order to minimize the SBL, the PSO strategy has been successively applied by setting $H = 1$, as in [30] [2], and $SBL^{ref} = -20\,dB$. Moreover, the following PSO setup has been chosen according to the guidelines in [51]: $S = 10$ particles, $w = 0.4$ (*inertial weight*), and $C_1 = C_2 = 2$ (*cognitive/social acceleration coefficient*).
At the convergence, after 500 iterations and $63.5\,[sec]$, the optimized values of the switch-on instants t^{on}_q, $q = 1, ..., Q$, are those given in Table 5.2 ($Q = 4$). Moreover, the plot of the pulse sequence is shown in Figure 5.4(a), while the corresponding patterns are displayed in Figure 5.4 (b). It is worth noticing that,

[2] Only the first harmonic mode has been optimized since the power loss reduces when the order of the harmonic mode increases.

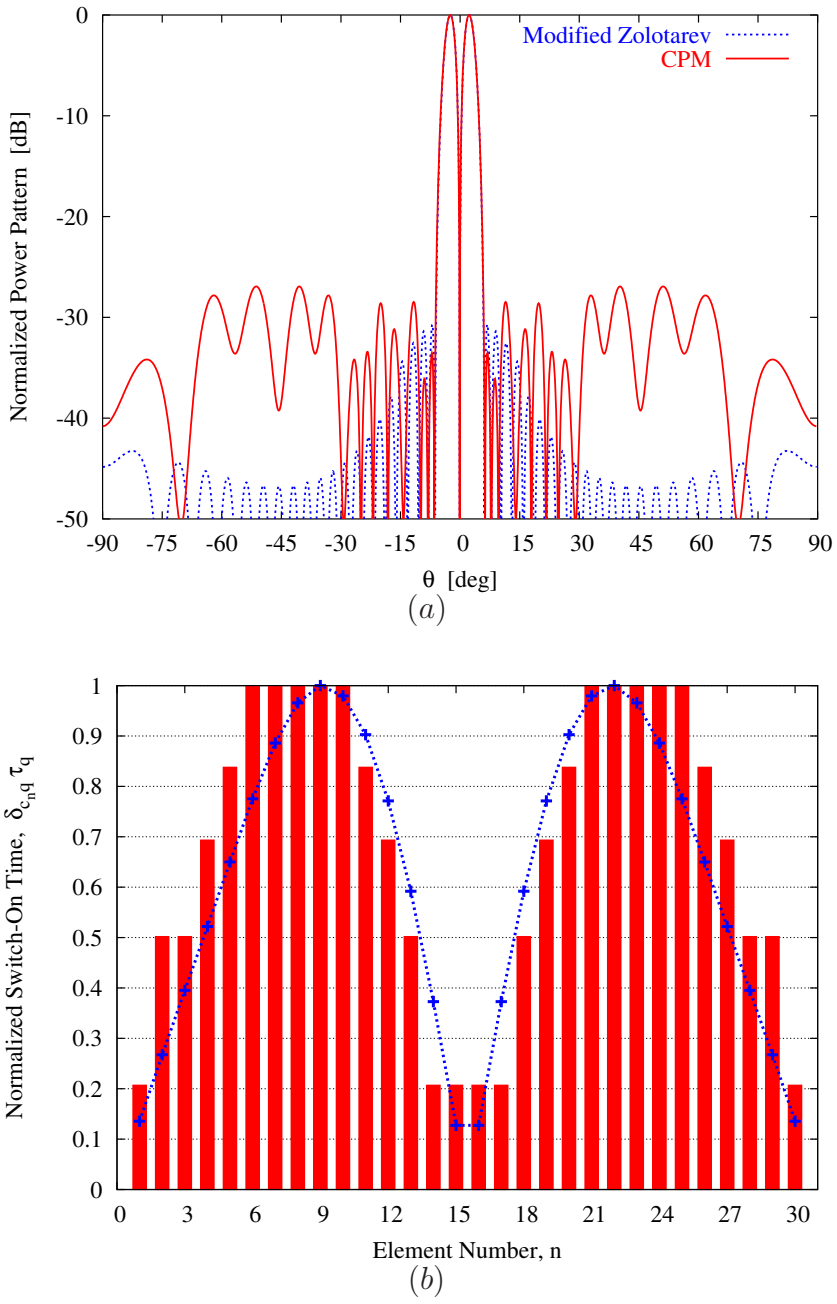

Figure 5.2: *Experiment 1* ($Q = 4$) - Plots of (a) the reference (Modified Zolotarev [35], $SLL = -30\,dB$, $\overline{n} = 5$) and CPM-synthesized power patterns at the carrier frequency ω_0 ($h = 0$) and (b) the corresponding switch-on times.

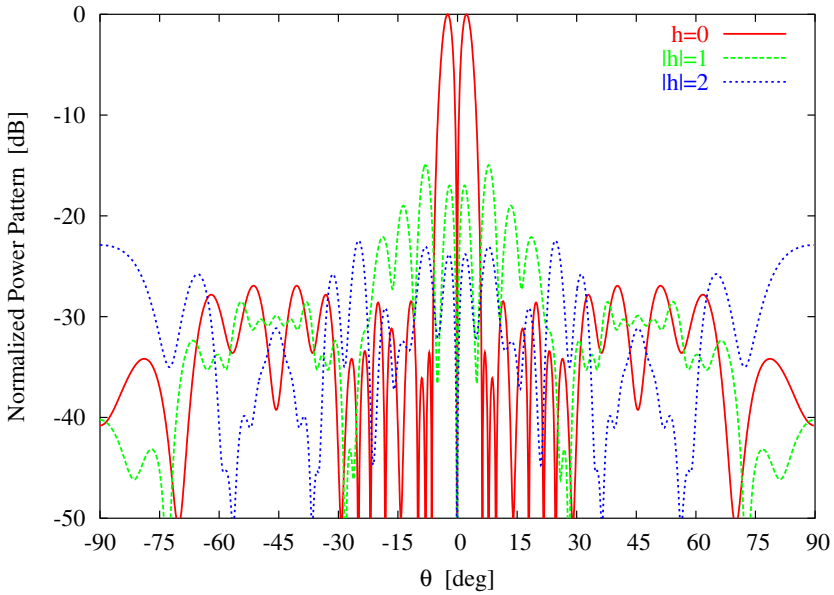

Figure 5.3: *Experiment 1* ($Q = 4$) - Normalized power patterns generated at ω_0 ($h = 0$) and $|h| = 1, 2$ by means of the CPM.

	$t_q^{on}\,[sec]$			
q	1	2	3	4
$Q = 4$	0.00	0.49	0.11	0.19
$Q = 2$	0.89	0.18	–	–

Table 5.2: PSO-optimized switch-on instants for the compromise difference patterns when $Q = 4$ and $Q = 2$.

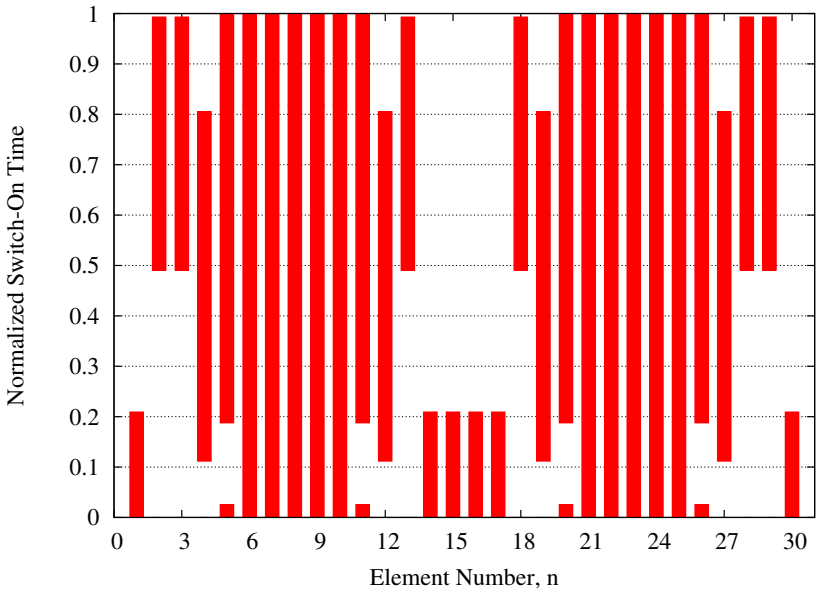

(a)

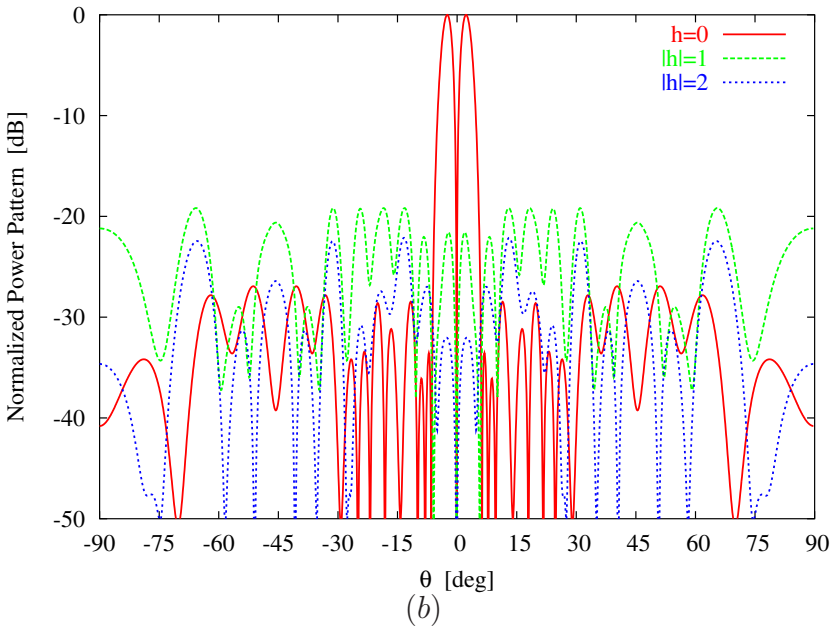

(b)

Figure 5.4: *Experiment 1* $(Q = 4)$ - *PSO*-optimization: (a) switch-on times and (b) power patterns at $|h| = 1, 2$.

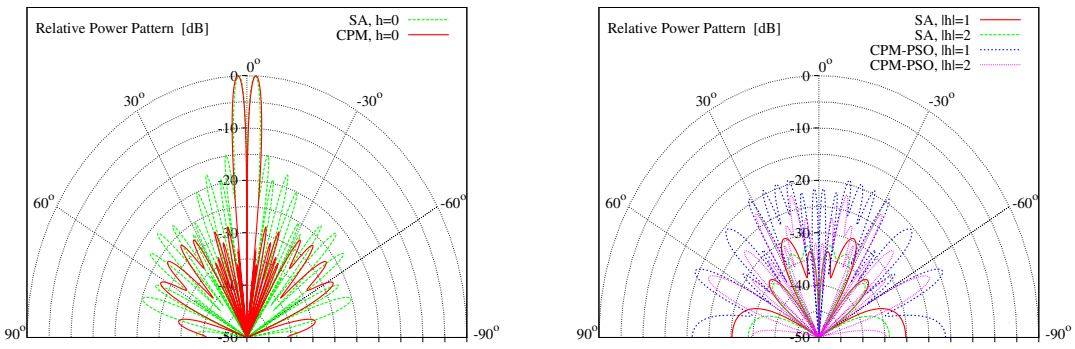

(a) (b)

Figure 5.5: *Experiment 1* $(Q = 4)$ - (a) Normalized difference power patterns at ω_0 $(h = 0)$ synthesized through the SA [30] and the $CPM - PSO$. (b) Polar plots of the corresponding sideband radiations at $|h| = 1, 2$.

without additional hardware, but simply adjusting the on-off sequence of the RF switches, the $SBL^{(1)}_{CPM}$ value is lowered of more than $4\,dB$ (i.e., $SBL^{(1)}_{CPM-PSO} = -19.2\,dB$ vs. $SBL^{(1)}_{CPM} = -14.9\,dB$). It is worth noting that neglecting the small "on-time interval" at the beginning of the period T_p for elements 5, 11, 20 and 26 [Figure 5.4(a)] the features of both the main pattern at central frequency and the harmonic patterns slightly modify (e.g., the SLL and the $SBL^{(1)}$ increase of $0.3\,dB$ and $0.5\,dB$, respectively). This fact would avoid these small intervals to be the bottleneck of the time-modulation system, allowing the RF switches to have less restrictions about their switch-on-to-switch-off speed.
For completeness, although the comparison is not completely fair since different synthesis problem are at hand, the solutions obtained with the $CPM-PSO$ and those shown in [30] are then analyzed by comparing the corresponding patterns at both the carrier frequency [Figure 5.5 (a)] and when $|h| = 1$, 2 [Figure 5.5(b)]. The power losses due to SRs, quantified through the close form relationship in [5], amounts to $P_{SR} = 21.3\%$ of the total radiated power in correspondence with the $CPM - PSO$. Otherwise ([30] - Tab. 4, Case B), the wasted power is only $P^{SA}_{SR} = 3\%$ and the SBL is much smaller [Figure 5.5(b)] since only $N^{SA}_{TM} = 8$ elements are time-modulated (instead of $N^{CPM}_{TM} = 20$). On the other hand, the efficiency of the $PSO-CPM$ approach in minimizing the SLL of the compromise difference patterns $(h = 0)$ is non-negligible [Figure 5.5(b)] ($SLL^{SA} = -14.9\,dB$ vs. $SLL^{CPM} = -26.9\,dB$).
In the second experiment (*Experiment 2*), the number of control elements is reduced by considering $R = 4$ RF switches ([30] - Tab. 4, Case C). The sum pattern is a Villeneuve pattern with $SLL = -20\,dB$, $\overline{n} = 3$, and $\nu = 1$ [35]. Moreover, the reference difference set $\mathbf{B}$ has been selected to generate a Modified Zolotarev difference pattern [35] with $SLL = -20\,dB$ and $\overline{n} = 4$.

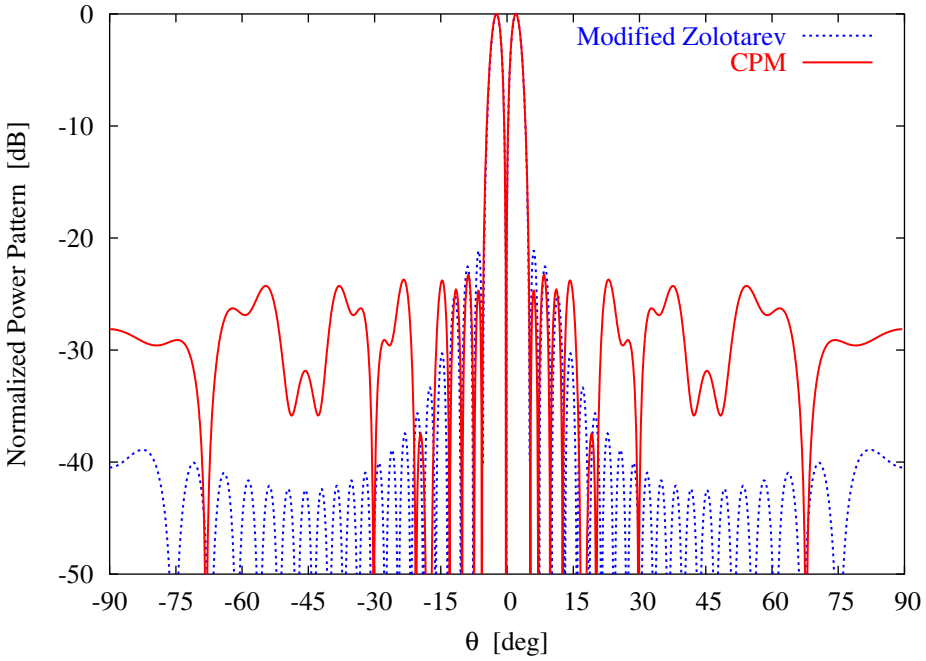

Figure 5.6: *Experiment 2* ($Q = 2$) - Plots of (a) the reference (Modified Zolotarev [35], $SLL = -20\,dB$, $\overline{n} = 5$) and CPM-synthesized power patterns at the carrier frequency ω_0 ($h = 0$).

Figure 5.6 shows the approximated pattern synthesized at the convergence of the CPM-based matching procedure by applying the pulse sequence $\mathbf{T}^{CPM}$ in Figure 5.7. The corresponding sub-array configuration is given in Table 5.1, as well. As for the first experiment, the secondary lobes do not decrease when θ grows [Figure 5.6], but the SLL value of the compromise pattern turns out to be lower than that of the Zolotarev one ($SLL^{CPM} = -23.3\,dB$ vs. $SLL^{ref} = -21.0\,dB$). Moreover, the same beamwidth has been achieved ($BW^{ref} = 2.36^o\,[deg]$ and $BW^{CPM} = 2.37^o\,[deg]$). Concerning the computational burden, 5 CPM iterations and $\sim 10^{-6}\,[sec]$ are enough to find the final solution.

Successively, the $SBL^{(1)}$ has been minimized by optimizing $\mathbf{T}^{on}$ with a PSO swarm of $S = 5$ particles. For comparison purposes, Figure 5.8 shows the patterns at $|h| = 0, 1, 2$ synthesized with the CPM and after the PSO optimization. Despite the reduced number of sub-arrays ($Q = 2$), the value of $SBL^{(1)}_{CPM} = -17.3\,dB$ has been reduced to $SBL^{(1)}_{CPM-PSO} = -19.3\,dB$ in $7.25\,[sec]$ after 100 iterations by defining the values of the final switch-on instants reported in Table 5.2.

For completeness, the $CPM-PSO$ patterns and those in [30] with four switches are shown in Figure 5.9(a) ($h = 0$) and Figure 5.9(b) ($|h| = 1, 2$). As regards to the number of time-modulated elements, it results that $N^{CPM}_{TM} = 10$ and $N^{SA}_{TM} =$

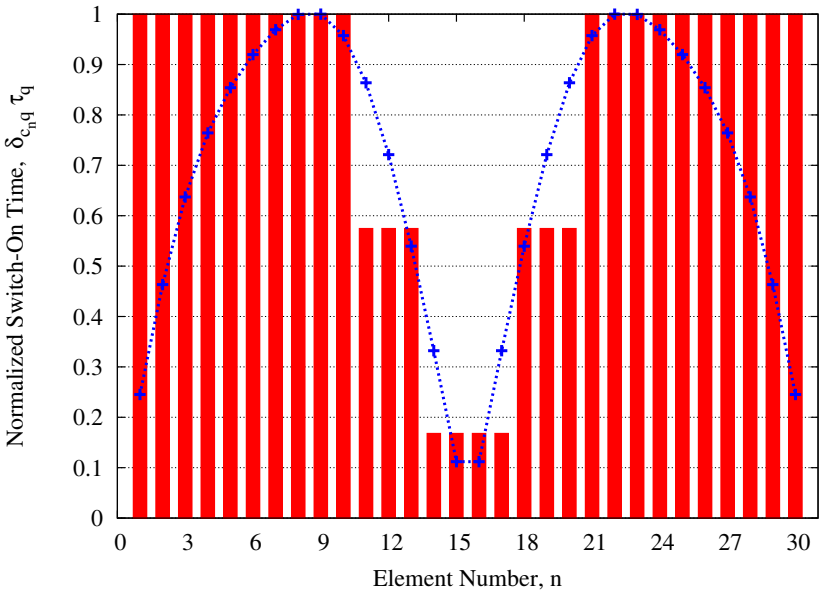

Figure 5.7: *Experiment 2* ($Q = 2$) - Switch-on times generating the pattern reported in Figure 5.6.

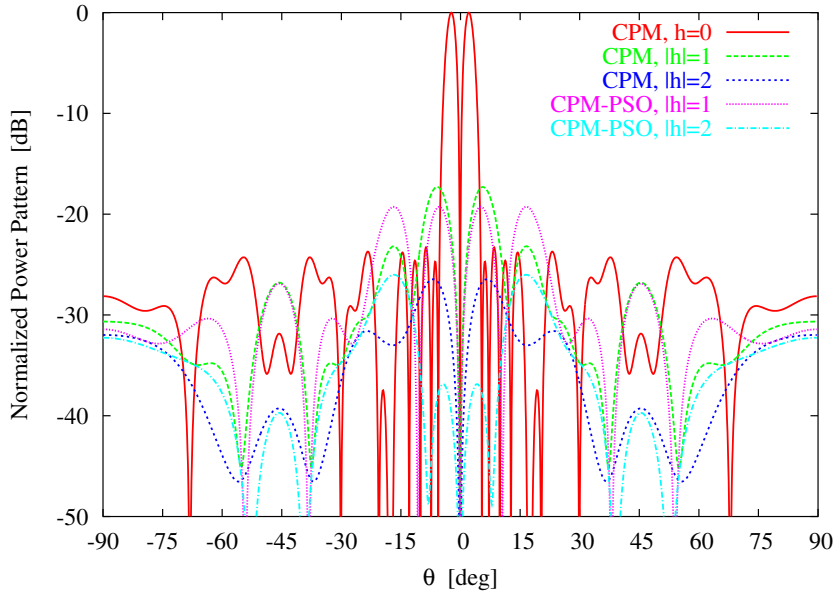

Figure 5.8: *Experiment 2* ($Q = 2$) - Normalized power patterns at ω_0 ($h = 0$) and $|h| = 1, 2$ synthesized by means of the CPM and the $CPM - PSO$ approach.

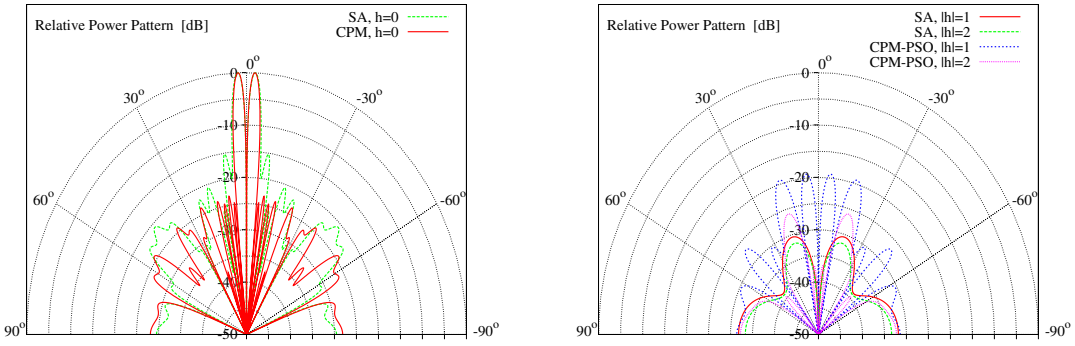

(a) (b)

Figure 5.9: *Experiment 2* ($Q = 2$) - (a) Normalized difference power patterns at ω_0 ($h = 0$) synthesized through the SA [30] and the $CPM - PSO$. (b) Polar plots of the corresponding sideband radiations at $|h| = 1, 2$.

4. Consequently, $P_{SR}^{CPM} = 16.9\%$ and $P_{SR}^{SA} = 2.1\%$, while $SLL^{CPM} = -23.3\,dB$ and $SLL^{SA} = -15.2\,dB$.

5.4 Discussions

In this chapter the potentialities of the time-modulation when dealing with the synthesis of monopulse sub-arrayed antennas have been investigated. Starting from a set of static excitations generating an optimal sum pattern, the signals at the sub-arrayed feed network have been time-modulated to generate a compromise difference pattern. Both the sub-array configuration and the duration of the time-pulse at each sub-array have been optimized solving a pattern matching problem by means of the CPM. Successively, a strategy based on the Particle Swarm Optimizer has been performed to minimize the SBL of the sideband radiations.

The obtained numerical results seem to indicate that the proposed approach is a interesting alternative for the synthesis of compromise sum and difference patterns. As a matter of fact, the main advantages of the proposed approach regard the reduced complexity of the antenna system and the possibility to change the shape of the beam pattern properly modifying the pulse sequence at the sub-array port.

Chapter 6

Conclusions and Future Developments

In this last chapter, some conclusions are drawn and further advances are envisaged in order to address the possible developments of the proposed technique.

In this thesis the synthesis of time-modulated antenna arrays has been investigated. In detail, the attention has been focused (*i*) on the review and the formulation of the equations describing the antenna array behavior when the time is exploited as additional degree of freedom into the synthesis problem, (*ii*) on the reduction of the power wasted due to the undesired harmonics and (*iii*) on the application of the time-modulation in the synthesis of compromise difference beams in monopulse arrays.

Thanks to an accurate analysis of the problem, the parameters involved in the sideband radiations are properly identified and such a knowledge is fully exploited to develop suitable strategies based on the global optimizer PSO aimed to minimize the power wasted by the undesired harmonics.

A set of representative examples concerned with the reduction of the sideband radiations SRs and the computation of the pulse sequences modulating the static excitations of the array have been reported in order to assess the effectiveness and flexibility of the proposed strategy. Comparison with other state-of-art techniques have been shown and discussed, as well.

Concerning the methodological novelties of this work, the main contributions consider the following issues:

- a full investigation of the behavior of time-modulated linear arrays during the pulse modulation;
- a proper identification of the parameters involved in the generation of the sideband radiations;
- the development of an innovative strategy based on the PSO that allows the minimization of the $SBLs$ in time-modulated linear arrays, optimizing the switch-on instants;
- the improvement of the algorithm minimizing the SRs, by means of the full expoitation of a closed-form relationship computing the total power wasted by the undesired harmonics and of the stochastic optimizer PSO;
- the derivation of an explicit expression that computes the wasted power in time-modulated planar arrays and the development of an effective approach aimed to reduce the SRs;
- the extension of the use of time to modulated the array excitations to synthetize a "best-compromise" difference pattern in sub-arrayed monopulse antennas.

As far as the future developments are concerned, there are many scenarios in which the potentialities of time-modulation in the antenna synthesis problems have been partially addressed.

As a matter of fact, the time-modulation seems to be a promising tool to generate multiple beams on the same antenna aperture. In such a framework, the

usually undesired sideband radiations arising from the periodic time-modulation of the static excitations of the array colud be profitably exploited to design an antenna system providing simultaneous multiple patterns

Moreover, since the modification of the shape of the radiated pattern in a time-modulated array can be performed easily, those devices can be properly used in noisy environments. In detail, the pulse sequence controlling the static element excitations can be reconfigured to maximize the signal-to-interference-plus-noise ratio at the receiver.

Moreover, the reduction of the power losses in linear time-modulated monopulse antenna can be enhanced using the explicit form describing the power radiated by the undesired harmonics. Finally, the planar geometry in time-modulated monopulse antenna should be taken into account.

References

[1] H. E. Shanks and R. W. Bickmore, "Four-dimensional electromagnetic radiators," *Canad. J. Phys.,* vol. 37, pp. 263-275, 1959.

[2] H. E. Shanks, "A new technique for electronic scanning," *IRE Trans. Antennas Propag.,* vol. AP-9, pp. 162-166, Mar. 1961.

[3] W. H. Kummer, A. T. Villeneuve, T. S. Fong, and F. G. Terrio, "Ultra-low sidelobes from time-modulated arrays," *IEEE Transaction on Antennas and Propagation,* vol. 11, pp. 633-639, 1963.

[4] R. W. Bickmore, "Time versus space in antenna theory," in *Microwave Scanning Antennas*, R. C. Hansen, Ed. Los Altos, CA: Peninsula, 1985, vol. III, ch. 4.

[5] J. C. Brégains, J. Fondevila, G. Franceschetti, and F. Ares, "Signal radiation and power losses of time-modulated arrays," *IEEE Transaction on Antennas and Propagation*, vol. 56, no. 6, pp. 1799-1804, Jun. 2008.

[6] W. Johler, "RF perfomance of ultra-miniature high frequency relays," in *Proceedings of* 49^{th} *IEEE Holm Conference on Electrical Contacts*, Washington D.C. USA, 8-10 Sept. 2003, pp. 298-301, Mar. 2004.

[7] "Understanding RF/Microwave solid state switches and their applications," Agilent Technologies, Inc. Application Note, 5989-7618, http://cp.literature.agilent.com/litweb/pdf/5989-7618EN.pdf.

[8] S. Yang, Y. B. Gan, and A. Qing, "Sideband suppression in time-modulated linear arrays by the differential evolution algorithm," *IEEE Antennas and Wireless Propagation Letters,* vol. 1, pp. 173-175, 2002.

[9] S. Yang, Y. B. Gan, and P. K. Tan, "A new technique for power-pattern synthesis in time-modulated linear arrays," *IEEE Antennas and Wireless Propagation Letters*, vol. 2, pp. 285-287, 2003.

[10] S. Yang, Y. B. Gan, and A. Qing, "Low sidelobe phased array antennas with time modulation," *IEEE Antennas and Propagation Society International Symposium,* Jun. 22-27, 2003.

[11] S. Yang, Y. B. Gan, and P. K. Tan, "Linear antenna arrays with bidirectional phase center motion," *IEEE Transaction on Antennas and Propagation,* vol. 53, no. 5, pp. 1829-1835, May 2005.

[12] J. Fondevila, J. C. Brégains, F. Ares, and E. Moreno, "Optimizing uniformly excited linear arrays through time modulation," *IEEE Antennas and Wireless Propagation Letters*, vol. 3, pp. 298-301, 2004.

[13] S. Yang, Y. B.Gan, A. Qing, and P. K. Tan, "Design of a uniform amplitude time modulated linear array with optimized time sequences," *IEEE Transaction on Antennas and Propagation,* vol. 53, no. 7, pp. 2337-2339, Jul. 2005.

[14] J. C. Brégains, J. Fondevila, G. Franceschetti, and F. Ares, "A first insight into the analysis of signal transmission and power losses in time-modulated linear arrays," *IEEE Antennas and Propagation Society International Symposium*, Washington, DC, pp. 831-834, Jul. 8-8, 2005.

[15] A. Tennant and B. Chambers, "A two-element time-modulated array with direction-finding properties," *IEEE Antennas and Wireless Propagation Letters*, vol. 6, pp. 64-65, 2007.

[16] A. Tennant and B. Chambers, "Direction finding using a four-element time-switched array system," *Antennas & Propagation Conference*, Loughborough, UK, pp. 181-184, Mar. 2008.

[17] A. Tennant and B. Chambers, "Time-switched array of phase-switched screens," *IEEE Transaction on Antennas and Propagation,* vol. 57, no. 3, pp. 808-812, Mar. 2009.

[18] J. Kennedy, R. C. Eberhart, and Y. Shi, *Swarm Intelligence*, San Francisco, CA: Morgan Kaufmann, 2001.

[19] M. I. Skolnick, *RADAR Handbook*, Third Edition, McGraw-Hill, 2008.

[20] D. A. McNamara, "Synthesis of subarrayed monopulse linear arrays through matching of independently optimum sum and difference excitations," *IEE Proceeding H.*, vol. 135, no. 5, pp. 371-374, Oct. 1988.

[21] L. Manica, P. Rocca, A. Martini, and A. Massa ,"An innovative approach based on a tree-searching algorithm for the optimal matching of independently optimum sum and difference excitations," *IEEE Transaction on Antennas and Propagation*, vol. 56, no. 1, pp. 58-66, Jan. 2008.

[22] Y. Chen, S. Yang, G. Li, and Z. Nie, "Adaptive nulling in time-modulated antenna arrays," *8th International Symposium on Antennas, Propagation and EM Theory, 2008*, Kunming, China, pp. 713-716, Nov. 2-5, 2008.

[23] J. Robinson , and Y. Rahmat-Samii, "Particle swarm optimization in electromagnetics", *IEEE Transaction on Antennas and Propagation,* vol. 52, no. 2, pp. 397-407, Feb. 2004.

[24] R. J. Mailloux, *Phased Array Antenna Handbook*, 2nd Ed. Norwood, MA: Artech House, 2005.

[25] A. Tennant and B. Chambers, "Control of the harmonic radiation patterns of time-modulated antenna arrays," *IEEE Antennas and Propagation Society International Symposium*, S. Diego, California, USA, July 5-12, 2008.

[26] C. L. Dolph, "A current distribution for broadside arrays which optimizes the relationship between beam-width and sidelobe level," *Proceedings IRE*, vol. 34, pp. 335-348, 1946.

[27] M. Donelli and A. Massa, "A computational approach based on a particle swarm optimizer for microwave imaging of two-dimensional dielectrical scatterers," *IEEE Transaction on Microwave Theory Techniques*, vol. 53, no. 5, pp. 1761-1776, May. 2005.

[28] S. Yang, Y. B. Gan, A. Qing, and P. K. Tan, "Evaluation of directivity and gain for time-modulated linear antenna arrays," *Microwave and Optical Technology Letters*, vol. 42, no. 2, pp. 167-171, Jul. 2004.

[29] G. Li, S. Yang, and Z. Nie, "A study on the application of time modulated antenna arrays to airborne pulsed doppler radar," *IEEE Transaction on Antennas and Propagation*, vol. 57, no. 5, pp. 1578-1582, May 2009.

[30] J. Fondevila, J. C. Brégains, F. Ares, and E. Moreno, "Application of time modulation in the synthesis of sum and difference patterns by using linear arrays," *Microwave and Optical Technology Letters*, vol. 48, no. 5, pp. 829-832, May 2006.

[31] T. T. Taylor, "Design of a circular aperture for narrow beamwidth and low sidelobes," *IRE Transaction on Antennas and Propagation*, vol. 8, pp. 17-22, 1960.

[32] R. S. Elliott, *Antenna Theory and Design,* Ed. Wiley, 2003.

[33] D. A. McNamara, "Direct synthesis of optimum difference patterns for discrete linear arrays using Zolotarev distribution," *IEE Proceeding H Microwave and Antennas Propagation*, vol. 140, no. 6, pp. 445-450, June 1993.

[34] A. T. Villeneuve, "Taylor patterns for discrete arrays," *IEEE Transaction on Antennas and Propagation*, vol. 32, no. 10, 1984, 32, pp. 1089-1093, Oct. 1984.

[35] D. A. McNamara, "Discrete $\bar{n}$-distributions for difference patterns," *Electronic Letters*, vol. 22, no. 6, pp. 303-304, June 1986.

[36] T. Isernia, P. Di Iorio, and F. Soldovieri, "An effective approach for the optimal focusing of array fields subject to arbitrary upper bounds," *IEEE Transaction on Antennas and Propagation*, vol. 48, no. 12, pp. 1837-1847, Dec. 2000.

[37] O. M. Bucci, M. D'Urso, and T. Isernia, "Optimal synthesis of difference patterns subject to arbitrary sidelobe bounds by using arbitrary array antennas," *IEE Proceeding Microwave Antennas Propagation*, vol. 125, no. 3, pp. 129-137, Mar. 2005.

[38] P. J. Bevelacqua, and C. A. Balanis, "Minimum sidelobe levels for linear arrays," *IEEE Transaction on Antennas and Propagation*, vol. 55, no. 12, pp. 3442-3449, Dec. 2007.

[39] T.-S. Lee, and T-K. Tseng, "Subarray-synthesized low-side-lobe sum and difference patterns with partial common weights," *IEEE Transaction on Antennas and Propagation*, vol. 41, no. 6, pp. 791-800, June 1993.

[40] T. T. Taylor, "Design of line-source antennas for narrow beam-width and low side lobes," *Transaction IRE*, vol. 3, pp. 16-28, 1955.

[41] E. T. Bayliss, "Design of monopulse antenna difference patterns with low sidelobes," *Bell System Technical Journal*, vol. 47, pp. 623-640, 1968.

[42] M. Alvarez-Folgueiras, J. A. Rodriguez-Gonzalez, F. Ares-Pena, "Synthesising Taylor and Bayliss linear distributions with common aperture tail," *Electronic Letters*, vol. 45, no. 1, pp. 18-19, Jan. 2009.

[43] F. Ares, S. R. Rengarajan, J. A. Rodriguez, and E. Moreno, "Optimal compromise among sum and difference patterns," *Journal of Electromagnetic Waves Application*, vol. 10, p. 1143-1555, Oct. 1996.

[44] P. Lopez, J. A. Rodriguez, F. Ares, and E. Moreno, "Subarray weighting for difference patterns of monopulse antennas: Joint optimization of subarray configurations and weigths," *IEEE Transaction on Antennas and Propagation*, vol. 49, no. 11, pp.1606-1608, Nov. 2001.

[45] S. Caorsi, A. Massa, M. Pastorino, and A. Randazzo, "Optimization of the difference patterns for monopulse antennas by a hybrid real/integer-coded differential evolution method," *IEEE Transaction on Antennas and Propagation*, vol. 53, no. 1, pp. 372-376, Jan. 2005.

[46] Y. Chen, S. Yang, and Z. Nie, "The application of a modified differential evolution strategy to some array pattern synthesis problems," *IEEE Transaction on Antennas and Propagation*, vol. 56, no. 7, pp.1919-1927, July 2008.

[47] M. D'Urso, T. Isernia, and E. F. Meliadò, "An effective hybrid approach for the optimal synthesis of monopulse antennas," *IEEE Transaction on Antennas and Propagation*, vol. 55, no. 4, pp. 1059-1066, Apr. 2007.

[48] P. Rocca, L. Manica, and A. Massa, "Hybrid approach for sub-arrayed monopulse antenna synthesis," *Electronic Letters*, vol. 44, no. 2, pp. 75-76, Feb. 2008.

[49] D. A. McNamara, "Synthesis of sum and difference patterns for two-section monopulse arrays," *IEE Proceeding H Microwaves Antennas Propagation*, vol. 135, no. 6, pp. 371-374, Dec. 1988.

[50] S. M. Sherman, *Monopulse Principles and Techniques*, Artech House, 1984.

[51] M. Donelli, G. Franceschini, A. Martini, and A. Massa, "An integrated multiscaling strategy based on a particle swarm algorithm for inverse scattering problems," *IEEE Transaction on Geoscience on Remote Sensing*, vol. 44, no. 2, pp. 298-312, Feb. 2006.

[52] I. S. Gradshteyn, and I. M. Ryzhik, *Table of Integrals, Series and Products*, Academic Press, 2000.

[53] A. W. Rudge, K. Milne, A. D. Oliver, and P. Knight, *The handbook of antenna design*, IEE Electromagnetic Waves Series, 1986.

Appendix A

Power of Sideband Radiation

This appendix is aimed at showing more details about the derivation of the explicit form that computes the power losses related to the sideband radiations, reported in Equation 4.14. For sake of clarity let us report here equation 4.12 :

$$\mathcal{P}_{SR} = \frac{1}{2}\int_0^{2\pi}\int_0^{\pi}\sum_{h=-\infty,h\neq 0}^{\infty}|\mu_h(\theta,\phi)|^2\sin\theta d\theta d\phi. \tag{A.1}$$

equation (4.9):

$$\mu_h(\theta,\phi) = \sum_{m=0}^{M-1}\sum_{n=0}^{N-1}\alpha_{mn}G_{mnh}e^{j\beta(x_m\cos\phi+y_n\sin\phi)} \tag{A.2}$$

and equation (4.13) [5]:

$$\sum_{h=-\infty,h\neq 0}^{\infty}G_{mnh}G_{rsh} = \Delta\tau_{mn}^{rs} - \tau_{mn}\tau_{rs} \tag{A.3}$$

Substituing (A.2) and (A.3) in (A.1), after simple algebra $\mathcal{P}_{SBR}$ turns out to be:

$$\begin{aligned}\mathcal{P}_{SR} \;=\; & \tfrac{1}{2}\sum_{m=0}^{M-1}\sum_{n=0}^{N-1}\sum_{r=0}^{M-1}\sum_{s=0}^{N-1}Re\left\{\alpha_{mn}\alpha_{rs}^*\right\}\left(\Delta\tau_{mn}^{rs}-\tau_{mn}\tau_{rs}\right)\\ & \int_0^{2\pi}\int_0^{\pi}e^{j\beta\sin\theta[(x_m-x_r)\cos\phi+(y_n-y_s)\sin\phi]}\sin\theta d\theta d\phi.\end{aligned} \tag{A.4}$$

Then, let us consider the following integral I:

$$I = \int_0^{2\pi}\int_0^{\pi}e^{j\beta\sin\theta[(x_m-x_r)\cos\phi+(y_n-y_s)\sin\phi]}\sin\theta d\theta d\phi \tag{A.5}$$

For sake of brevity, let us rewrite (A.5) as:

$$I = \int_0^{\pi} I_\theta\sin\theta d\theta \tag{A.6}$$

where:

$$I_\theta = \int_{-\pi}^{\pi} e^{j(a\cos\phi + b\sin\phi)} d\phi \tag{A.7}$$

being $a = \beta \sin\theta\,(x_m - x_r)$ and $b = \beta \sin\theta\,(y_n - y_s)$. By considering the Euler's relationships:

$$\begin{aligned} a\cos\phi + b\sin\phi &= a\frac{\left(e^{j\phi}+e^{-j\phi}\right)}{2} + b\frac{\left(e^{j\phi}-e^{-j\phi}\right)}{2j} \\ &= \sqrt{a^2+b^2}\sin\left[\phi + \arctan\left(\tfrac{a}{b}\right)\right], \end{aligned} \tag{A.8}$$

and substituing (A.8) in (A.7) I_θ turns out to be:

$$I_\theta = \int_{-\pi}^{\pi} e^{j\sqrt{a^2+b^2}\sin\left[\phi + \arctan\left(\frac{a}{b}\right)\right]} d\phi \tag{A.9}$$

whose the closed-form solution in terms of Bessel functions is [52]:

$$I_\theta = 2\pi J_0\left(\sqrt{a^2+b^2}\right) \tag{A.10}$$

therefore, Equation (A.5) reduces to:

$$I = 2\pi \int_0^{\pi} J_0\left(\sqrt{a^2+b^2}\right)\sin\theta d\theta \tag{A.11}$$

or in its explicit form [53]:

$$I = 4\pi \frac{\sin\left(\beta\sqrt{(x_m - x_r)^2 + (y_n - y_s)^2}\right)}{\left(\beta\sqrt{(x_m - x_r)^2 + (y_n - y_s)^2}\right)} \tag{A.12}$$

then, substituing (A.12) in (A.4), the closed-form relationship describing the total power radiated by the sideband radiations is:

$$\begin{aligned} \mathcal{P}_{SR} &= 2\pi \sum_{m=0}^{M-1}\sum_{n=0}^{N-1}\sum_{r=0}^{M-1}\sum_{s=0}^{M-1} \Big[Re\left\{\alpha_{mn}\alpha_{rs}^*\right\} \cdot \\ &\quad \cdot \frac{\sin\left(\beta\sqrt{(x_m-x_r)^2+(y_n-y_s)^2}\right)}{\beta\sqrt{(x_m-x_r)^2+(y_n-y_s)^2}} \left(\Delta\tau_{mn,rs} - \tau_{mn}\tau_{rs}\right)\Big] \end{aligned} \tag{A.13}$$